HHS Public Access

Author manuscript

J Tissue Eng Regen Med. Author manuscript; available in PMC 2019 May 09.

Published in final edited form as:

J Tissue Eng Regen Med. 2018 November ; 12(11): 2203–2220. doi:10.1002/term.2744.

Ionic silicon improves endothelial cells' survival under toxic oxidative stress by overexpressing angiogenic markers and antioxidant enzymes

Felipe Monte[1,2], **Tugba Cebe**[1], **Daniel Ripperger**[3], **Fareed Ighani**[3], **Hristo V. Kojouharov**[4], **Benito M. Chen**[4], **Harry K. W. Kim**[2,5], **Pranesh B. Aswath**[6], and **Venu G. Varanasi**[6,7]

[1]Department of Bioengineering, University of Texas at Arlington, Arlington, Texas

[2]Center for Excellence in Hip Disorders, Texas Scottish Rite Hospital, Dallas, Texas

[3]Texas A&M University College of Dentistry, Dallas, Texas

[4]Department of Mathematics, University of Texas at Arlington, Arlington, Texas

[5]Department of Orthopedic Surgery, University of Texas Southwestern Medical Center at Dallas, Dallas, Texas

[6]Department of Materials Science and Engineering, University of Texas at Arlington, Arlington, Texas

[7]Department of College of Nursing and Health Innovation, University of Texas at Arlington, Arlington, Texas

Abstract

Oxidative stress, induced by harmful levels of reactive oxygen species, is a common occurrence that impairs proper bone defect vascular healing through the impairment of endothelial cell function. Ionic silicon released from silica-based biomaterials, can upregulate hypoxia-inducible factor-1α (HIF-1α). Yet it is unclear whether ionic Si can restore endothelial cell function under oxidative stress conditions. Therefore, we hypothesized that ionic silicon can help improve human umbilical vein endothelial cells' (HUVECs') survival under toxic oxidative stress. In this study, we evaluated the ionic jsilicon effect on HUVECs viability, proliferation, migration, gene expression, and capillary tube formation under normal conditions and under harmful hydrogen peroxide levels. We demonstrated that 0.5-mM Si^{4+} significantly enhanced angiogenesis in HUVECs under normal condition ($p < 0.05$). HUVECs exposed to 0.5-mM Si^{4+} presented a morphological change, even without the bed of Matrigel, and formed significantly more tube-like structures than the control ($p < 0.001$). In addition, 0.5-mM Si^{4+} enhanced cell viability in HUVECs under harmful H_2O_2 levels. HIF-1α, vascular endothelial growth factor-A, and vascular endothelial growth factor receptor-2 were overexpressed more than twofold in silicon-treated HUVECs, under normal and toxic H_2O_2 conditions. Moreover, the HUVECs were treated with 0.5-mM Si^{4+} overexpressed superoxide

Correspondence: Venu G. Varanasi, College of Nursing and Health Innovation, University of Texas at Arlington, 411 S. Nedderman Drive, Arlington, TX 76019-0407. venu.varanasi@uta.edu.

CONFLICT OF INTEREST

The authors have declared that there is no conflict of interest.

dismutase-1 (SOD-1), catalase-1 (Cat-1), and nitric oxide synthase-3 (NOS3) under normal and oxidative stress environment ($p < 0.01$). A computational model was used for explaining the antioxidant effect of Si^{4+} in endothelial cells and human periosteum cells by SOD-1 enhancement. In conclusion, we demonstrated that 0.5-mM Si^{4+} can recover the HUVECs' viability under oxidative stress conditions by reducing cell death and upregulating expression of angiogenic and antioxidant factors.

Keywords

angiogenesis; angiogenic markers; antioxidant enzymes; cell survival; endothelial cells; ionic silicon; oxidative stress

1 | INTRODUCTION

One million bone graft procedures are performed in the United States every year (Vacanti & Langer, 1999). Many of these procedures are used to correct large bone defects that are a hypoxic environment, rich in reactive oxygen species (ROS). The high levels of ROS create an oxidative stress that can damage the cells and make it difficult to enable adequate tissue regeneration (Ryter et al., 2007; Tabak et al., 2011). Hence, biomaterials have been used as bone substitute for treatment of these injuries. However, despite all the advances in bone tissue engineering, there are limitations in the ability to address the repair of large bone defects with a suitable biomaterial that can meet the requirements of biocompatibility and osteointegration. Moreover, there is limited understanding about the role played by these biomaterials in the healing area under oxidative stress induced by the deleterious hypoxic conditions.

There is remarkable evidence of silicon's effect in bone formation (Asselin et al., 2004; Hench, Splinter, Allen, & Greenlee, 1971; Ilyas, Lavrik, Kim, Aswath, & Varanasi, 2015; Lu, Marcucio, & Miclau, 2006; Odatsu et al., 2015; Renno et al., 2013; Ryter et al., 2007; Tabak et al., 2011; Varanasi et al., 2012; D. Wang et al., 2014). Silicon-based and Si-doped materials have been used as biomaterials to enhance bone regeneration, as they elicit mineral deposition and osteoblast differentiation (Ilyas et al., 2015; Odatsu et al., 2015). Currently, the biomaterials have been designed to act at a molecular level by stimulating a specific cellular response (Asselin et al., 2004). Since the 1970s, with the discovery of bioactive glass 45S5 (Bioglass®; Hench et al., 1971), these Si-based materials have been shown to enhance bone healing and material-bone attachment through Si^{4+} and Ca^{2+} release, inducing deposition of a hydroxycarbonate apatite layer within a few hours (Renno et al., 2013), posterior osteoblast differentiation, and collagen type I deposition (Varanasi et al., 2012; D. Wang et al., 2014).

Angiogenesis is crucial for bone tissue repair (Lu et al., 2006) and involves endothelial cell's migration, proliferation, differentiation, and tube formation (Saghiri, Asatourian, Orangi, Sorenson, & Sheibani, 2015). The newly formed blood vessels transport the growth factors, cytokines, and progenitor cells to damaged tissue. A recent study correlated Si^{4+} release from mesoporous silica microspheres with hypoxia-inducible factor-1α (HIF1-α) up regulation (Dashnyam et al., 2017). Early on after trauma, tissue repair occurs in a hypoxic

environment, and changes in mitochondrial activity occur, leading to ROS' overproduction. Hypoxia can induce HIF-1α accumulation and angiogenesis downstream pathway activation (Solaini, Baracca, Lenaz, & Sgarbi, 2010). However, elevated levels of ROS create a cell-damaging effect that can impede proper endothelial cell function (Sharma, Jha, Dubey, & Pessarakli, 2012). The threshold among physiologic, angiogenic, and hazardous levels of ROS depends on the cell type. Although the mesenchymal stem cells are more sensitive to cell damage due to ROS, the endothelial cells have been shown to be more resilient (Wen et al., 2013). Thus, it appears that the early effect of silicon ion released from biomaterials needs to be understood to establish the role of this element in angiogenesis under deleterious levels of oxidative stress.

Human umbilical vein endothelial cells (HUVECs) are well established for the study of the angiogenic effect of drugs and biomaterials in vitro (Morin & Tranquillo, 2013; Sivaraman et al., 2017; X. Wang et al., 2016). ROS are described as reactive molecules and free radicals derived from molecular oxygen; products generated from metal catalysed oxygen reaction generated from mitochondrial activities. Under hypoxic conditions, the ROS levels can increase to concentrations that induce additional cellular damage. In particular, hydrogen peroxide is a major contributor to oxidative damage (Solaini et al., 2010). Large bone defects lead to hypoxia and production of deleterious levels of ROS. These conditions are usually present in regions surrounding implants and biopolymers used for biological and structural support of bone defects. The studies mentioned above support the idea that silicon ion can have a positive effect on bone healing in pro-oxidant conditions by enhancing HIF-1α and improving angiogenesis. However, there is no conclusive study that evaluates the isolated effect of the silicon ion on HUVECs under harmful levels of ROS. Therefore, this isolated effect is studied in this work.

Thus, we hypothesize that Si^{4+} at specific concentration(s) can enhance the HUVECs' viability in a toxic level of hydrogen peroxide by upregulating the gene expression of HIF-1α and, accordingly, vascular endothelial growth factor-A (VEGFA), and vascular endothelial growth factor receptor-2 (VEGFR-2). Our goal is to gain a new understanding of the silicon ion on HUVECs under harmful oxidative stress levels and understand the element's role in angiogenesis during the early stages of tissue repair. First, the cells' viability, proliferation, tube formation, and migration in HUVECs under normal condition (culture media without H_2O_2) are verified, using three different Si^{4+} concentrations (0.1, 0.5, and 1 mM). Second, the cell viability and gene expression on HUVECs exposed to toxic levels of H_2O_2 treated with specific(s) Si^{4+} ions concentration(s) are tested. We also investigated the effect of ionic silicon on gene expression of antioxidant, superoxide dismutase-1 (SOD-1), catalase-1 (Cat-1), and nitric oxide synthase-3 (NOS3) produced by endothelial cells. These oxidative stress markers play a relevant role in the reduction of deleterious oxidative stress and facilitation of angiogenesis and osteogenesis during the tissue-healing process (Choi, Lee, Chung, & Park, 2012; Diwan, Wang, Jang, Zhu, & Murrell, 2000; Fernández, San Miguel, & Fernández-Briera, 2009; Matsunaga et al., 2002; Murohara et al., 1998).

2 | MATERIAL AND METHODS

2.1 | Silicon ion and hydrogen peroxide solutions preparation

The Si^{4+} solution was prepared by dissolving sodium meta-silicate—Na_2SiO_3 (1 mol L – 1) 4 preparation, the solution was filtered using a nylon syringe filter (33 mm, 0.2 μm, 50/PK) and followed by serial dilutions until the final dilution in endothelial cell culture media-2 (Lonza Walkersville, In) reached the desired Si^{4+} concentrations: 0.1 0.5, and 1.0 mM. Hydrogen peroxide (H_2O_2 30% (*w/v*)) was used as the source of ROS and was diluted with sterile water followed by filtration, as mentioned above. Serial dilutions were made with sterile water until the desired H_2O_2 concentrations were reached: 0.2, 0.4, 0.6, 0.8, 1.0, and 1.5 mM. The last dilution was made in the well plate with the specific endothelial cell media.

2.2 | Cell culture

HUVECs (Lonza Walkersville, In) were thawed and subcultured in 75-cm^2 Corning® cell culture flasks with canted neck and vented caps following manufacturer's protocol (Technical Information, 2014). Endothelial cell growth media 2 (EGM-2; Lonza Walkersville, In) was used for the HUVECs' expansion, and the media was changed every 2 days until the cells reached 70% confluence. The HUVECs were then subcultured. Cells from Passage 3 were used on all the designed experiments.

2.3 | HUVECs' viability exposed to different H_2O_2 concentrations

A total of 3×10^4 cells/cm^2 were seeded per well in a 96-well plate using a total volume of 100 μl of specific cell culture media ($n = 12$ per group), depending on the study. Endothelial growth media (EGM) was used as control, and the other six groups were formed by the H_2O_2 concentrations detailed earlier. The sterile water with H_2O_2 was placed on the bottom of the well before the reduced EGM; this was prepared by diluting EGM with endothelial basal media (EBM) for a final concentration of 20% (*v/v*) and is labelled on this manuscript as EGM 20%, fetal bovine serum (FBS) concentration was corrected to 2% after dilution. Analyses were conducted after 6 and 24 hr, and six samples were used per time point for Calcein-AM (BD, Biosciences, CA) fluorescent staining, and six samples were used for CellTiter 96® AQueous One Solution Cell Proliferation Assay (MTS). First, the cells were prepared for the proliferation assay, and a solution was prepared using 1 ml of EBM per 100 μl of the reagent. After the specific time point, the cell culture media was removed from each well and 120 μl of the prepared solution was placed inside the well. After 3 hr, 60 μl of the solution was collected and placed in a new 96-well plate. This was read using a microplate reader POLARstar Omega BMG Labtech at a 490-nm wave length. Next, 50 μl of Calcein-AM 2 mM was added to the other six wells per group and allowed to sit for 30 min. Fluorescent pictures were taken using the Carl Zeiss Axio Vert A1 TL/RL LED Inverted Microscope with the light filter. All results presented were compared with the initial cell seeding density.

2.4 | Silicon ion effect on HUVECs under normal conditions (viability and proliferation)

2.4.1 | Cell viability—In all, 1.5×10^4 cells/cm^2 were seeded per well with $n = 12$ per group in the five groups: EBM + 0.1% FBS (negative control), EGM (positive control), EBM + 0.1% FBS + Si^{4+} 0.1 mM, EBM + 0.1% FBS + Si^{4+} 0.5 mM, and EBM + 0.1% FBS + Si^{4+} 1 mM. After 6 and 24 hr, six samples per group on each time point were used for the MTS assay.

2.4.2 | Cell proliferation—Totally, 1.5×10^4 cells/cm^2 were seeded per well with $n = 12$ per group in the five groups: EGM 20% (negative control), EGM (positive control), EGM 20% + Si 0.1 mM, EGM 20% + Si 0.5 mM, and EGM 20% + Si 1 mM. All groups with silicon ion were prepared with EGM 20%, with an aim to give more sensitivity to changes induced by the different Si^{4+} concentrations on HUVECs. In order to determine the best EGM dilution for this experiment, the cells were cultivated in EGM, diluted in three different concentrations. EGM at 20% dilution exhibited a significant difference ($p < 0.01$) in cell proliferation, relative to control after 24 hr. The data were collected using the same methods mentioned in Section 2.3 at 6, 24, and 48 hr after cell seeding, using the MTS assay ($n = 6$ per group each time point) and Calcein-AM fluorescent staining ($n = 6$ per group each time point) for pictures. Additionally, the fluorescent images were used for cell counting on ImageJ, v1.47 (National Institutes of Health, Bethesda, MD; Rasband, 1997).

2.5 | Capillary-like tube formation assay under different Si^{4+} concentrations

2.5.1 | HUVECs seeded on bed of Matrigel—The experimental design groups were the same as used in Section 2.4, with $n = 6$ per group. The experiment was conducted according to previous studies (Technical Information, 2014; Arnaoutova & Kleinman, 2010). Briefly, first, 50 μl of Matrigel® Matrix (Basement Membrane Phenol-Red Free) was placed at the bottom of each well and placed in an incubator at 37°C, with 95% relative humidity and 5% CO_2, for 30 min. Thereafter, 50,000/cm^2 cells were seeded per well, using 100 μl of specific media and/or Si^{4+}, as detailed above. The well plate was maintained in the incubator for 6 hr and was subsequently stained with Calcein-AM using the same method as mentioned in Section 2.3. Lastly, after 30 min, three different pictures were captured per well using Zeiss Fluorescent Microscopy FITC Filter at 5× magnification. The angiogenesis analyser ImageJ plugin (Rasband, 1997) was used for measuring the total tube length (pixels), number of nodes, number of meshes, and number of segments.

2.5.2 | HUVECs seeded in well plates without Matrigel—Four groups were used for capillary-like tube formation without Matrigel: EBM (control) and the three silicon ion concentrations (0.1, 0.5, and 1.0 mM); 50,000 cells/cm^2 were seeded per well ($n = 5$ per group) in a 96-well plate using 100 μl of EGM-2. After 24 hr, the growth media from three of the four groups was changed to media with three different silicon ion concentrations, and the final group was replaced with BASAL MEDIA to serve as the control. Three hours after the media change, the cells were stained with Calcein-AM, following the protocol described. Three different 5× magnification images were captured per well using Zeiss fluorescent microscopy; FITC filter and ImageJ were used for calculations. A number of connected networks formed, indicating that morphological change of HUVECs into capillary precursor structures is presented.

2.6 | Scratch wound healing assay

This experiment utilized three groups (n = 3 per group): EGM (positive control), EBM-2 (negative control), and Si^{4+} 0.5 mM + EBM (treatment). Initially, 50,000 cells were seeded in each well and cultured until they reached 90% cell confluence. A 200-μl pipette tip was used to make a scratch in a cross shape; the media was removed, and each well was washed two times with phosphate buffer solution (PBS). The new media was added according to the groups described above. A 5× magnification bright field image was taken just after the addition of the new media (t0). After 12 hr (t12), the wells were washed with PBS, fixed with 4% paraformaldehyde solution, and stained with toluidine blue. Images were captured from the same area as the t0 images, and the percentage of occupied area at t12 was calculated using the Wound Healing ImageJ software plugin (Rasband, 1997).

2.7 | Transwell migration assay

The cell migration by transwell membrane was tested in triplicate in the following groups: EGM (positive control), EBM + 2% FBS (negative control), and EBM + 2% FBS + Si^{4+} 0.5 mM (treatment). In all, 30,000 cells were seeded in the upper chamber of the 8-μM transwell (Castor Inc) in 100-μl EBM. Thereafter, 600 μl of studied media was placed at the bottom of the well, and the cells were allowed to migrate through the micropores for 12 hr; the HUVECs were fixed with 4% paraformaldehyde solution. After fixation, the cells from the upper part of the well were removed using a cotton swab, and the remaining cells (bottom/migrated cells) were stained with DAPI (P369, Invitrogen) for nuclear visualization. Finally, three images per well were captured at 5×, 10×, 20×, and 40× magnification view using Zeiss Fluorescent Inverted Microscopy, and ImageJ software was used for cell counting.

2.8 | Effect of Si^{4+} on HUVECs under harmful hydrogen peroxide level

2.8.1 | Cell viability—The Si^{4+} and H_2O_2 solutions and cells suspensions were prepared following the method mentioned in Sections 2.3 and 2.4. The experiment used three experimental groups: EGM, EGM + H_2O_2 0.6 mM, and EGM H_2O_2 0.6 mM + Si 0.5 mM (treatment). Both 0.6 mM H_2O_2 and Si^{4+} 0.5 mM were used, based on the results observed in the previous sections. Totally, 15,000 cells/cm^2 were seeded per well in a 96-well plate with 12 samples per group (n = 12). The data were collected after 6 and 24 hr. In all, six samples per group were used for the MTS assay, and six samples per group were used for live and dead fluorescent microscopy staining with Calcein-AM (3 μM) and propidium iodite (4.5 μM) diluted in warm DPBS. Analysed data are presented relative to control (EGM).

2.8.2 | Quantitative real-time polymerase chain reaction—In total, 500,000 cells were seeded in a six-well plate (n = 6 per group) and cultured for 24 hr. The experimental groups were the same used for viability (Section 2.8.1). First, the cells were lysed using the buffer RLT (guanidinum thiocyanate) with 10-μl β-Mercaptoethanol per 1 ml of buffer. Second, the cells were sheared using rubber scrapper under mild pressure to lyse the cells and collect mRNA (RNeasy Mini Kit, Qiagen, Valencia, CA, USA), which were then converted to cDNA using quantitative real-time polymerase chain reaction method (ReverseTranscription System, Promega, Madison, Wl, USA) according to manufacturer's

protocol. Both mRNA and cDNA were quantified during the process using microvolume UV-VIS spectrophotometer (Nano Drop 2000c, Thermo Fisher Scientific Inc., Watham, MA, USA). Reference gene 18S was used as housekeeping to be considered more specific to HUVEC cells (Chen et al., 2013), and GAPDH was also used as housekeeping for better comparison with other studies. Lastly, relative quantification of gene expression was evaluated by comparing the cycle threshold (CT) method and fold change, calculated using $2^{-\Delta\Delta CT}$. The studied genes included VEGFA, KDR or VEGFR-2, HIF1-α, SOD-1, Cat-1, and NOS3 and eNOS (Table 1). The data were calculated relative to the housekeeping genes and compared with control (EGM 20%).

2.9 | Statistical methods

The data of the experiments described above were expressed as means and standard deviations. Statistical analysis was performed using a one-way ANOVA with post hoc Tukey's Pairwise for comparison amongst all groups, and Student *t*-test for comparison between groups. The significant level was considered when $p < 0.05$. Past3 version 3.15 and OriginPro 2015 Statistical Softwares were used for calculations and graphs.

Sample size was determined based on the number of groups and standard deviation from the pilot study, and G*Power 3 version 3.0.5 Statistical Software was used for calculations.

A confidence interval of 95% and a statistical power of 80% for all required calculations were considered.

Analysed data are presented on bar graphs, cell viability, and proliferation under ROS environment, and normal condition is shown relative to initial cell seeding; cell migration assays are presented relative to positive control. The gene expression is shown relative to the housekeeping gene and compared with control. Capillary tube formation was not normalized.

2.10 | Computational model of ionic silicon and amorphous silica-based implants effect in superoxide dismutase expression and ROS reduction

2.10.1 | Fabrication and surface analysis of coated amorphous silica-based implants—Cylindrical surgical stainless-steel rods and planar substrate were cleaned by standard procedure. First, the implants were immersed in a piranha solution (3:1 mixture of sulfuric acid—H_2SO_4, 96%—and hydrogen peroxide—H_2O_2, 30%). Second, they were rinsed in deionized water. Third was their immersion in hydrofluoric acid to remove the native oxide layer. Finally, the implants were rinsed in deionized water for three cleaning cycles, dried with N_2 gas, and placed on 200°C hot plate (Ilyas et al., 2015; Ilyas et al., 2016).

A TRION ORION II PECVD/LPECVD System (TRION Technology, Clearwater, FL) was used to deposit a 1,000-nm uniform coating of SiON. All coatings were processed at a substrate temperature of 400°C, a chamber pressure of 900 mTorr, an inductively coupled plasma (ICP) power of 30 W, and an applied excitation frequency of 13.56 MHz. The source and flow rate of gas were as follows: 24 for SiH_4/AR (15/85%), 155 for N_2O, 225 for N_2, and 50 for NH_4 (Ilyas et al., 2015; Ilyas et al., 2016).

The implant coating used for ionic silicon release study was patterned using the method described in previous publications (Ilyas et al., 2015).

The coated rods were used for surface elemental analysis and coating thickness. The elemental surface composition was verified using energy dispersive X-ray analysis, mapping from scanning electron microscopy (SEM; Hitachi S-3000N Variable Pressure) at acceleration voltage of 12 KeV. The SEM was also used for verifying film thickness at 20 KeV.

2.10.2 | Si^{4+} release from implants and cell culture study—First, samples were fabricated/coated as mentioned in Section 2.10.1 using a 12 × 12 mm silicon wafer (NOVA Electronic Materials, 1189 Porter Rd. Flower Mound, TX, USA) and placed in 4 ml of cell culture medium (α-MEM) at 37°C and 5% CO_2, for 6 weeks without cells. The Si^{4+} concentration was measured using ICP optical emission spectrometry (ICP-OES, ICPE-9000, SHIMAZU Co., Kyoto, Japan) as described in previous publications (Ilyas et al., 2016). The study was conducted for 6 weeks, with a 1-week interval, and media change every 48 hr ($n = 3$). At the end, scanning electron microscopy (Hitachi S-3000N Variable Pressure SEM) was used for image acquisition and verification of possible hydroxyapatite deposition on coated implants.

Second, we tested the effect of PECVD-based silicon oxynitride overlay implants and ionic silicon in human periosteum cells (HPCs) and pig's aorta endothelial cells (PAECs), respectively. The HPCs were obtained according to previous protocol and the guidelines followed in IRB protocol (Study ID STU 012011–181; Kim, Oxendine, & Kamiya, 2013). The HPCs were cultured up to Passage 4 in growth medium (α-MEM + 10% FBS and 1% penicillin streptomycin [P/S]). Thereafter, we seeded 100,000 cells per well on implants and glass cover slip (control) using a six-well plate ($n = 3$). The cells were synchronized (α-MEM, 1% FBS, 1% pen-strep) for 48 hr. Then, the media was exchanged with growth media with 50 ppm ascorbic acid-2-phosphate (AA2P, Sigma-Aldrich Corp., St. Louis, MO, USA) and glycerol-2-phosphate (β-GP, Sigma-Aldrich Corp.) for differentiation. At 3 and 4 days after differentiation, the SOD-1 mRNA levels were measured according to the method described in previous publications (Ilyas et al., 2016; Odatsu et al., 2015). We used GAPDH as the housekeeping gene for measuring mRNA levels.

Lastly, we obtained PAECs from immature piglets. The cells were isolated from the aorta wall by a collagenase treatment, seeded on 1% porcine gelatin-coated plates, and cultured in supplemented medium (Gibco® RPMI1640 Media +10% FBS +1% PS + 2 mM L-glutamine +30-μg/ml endothelial cell growth factor) until Passage 3. The method used for measuring the SOD-1 mRNA levels in endothelial cells exposed to ionic silicon was described above in Section 2.8.2. For SEM images, we seeded 50,000 PAECs per well ($n = 3$) on uncoated silicon wafer (control) and on amorphous silica coating implants ($SiON_x$), using the same media used for cell growth, with 2% FBS. At the end, 24 hr after cell seeding, the media was removed, the cells were fixed in 2.5% glutaraldehyde, dehydrated in ethanol, dried at room temperature, and coated with silver for SEM analysis.

2.10.3 | Computational methods

The principal discrete models are the random, the ballistic, and the solid on solid. All these models allow the deposition of particles on the surface, their movement along the surface, and finally a stochastic partial differential equation for the height of the deposited surface as a function of time and position. These partial differential equations are simplified by neglecting certain terms, to obtain a Langevin equation with a multidimensional Gaussian stochastic process noise term (Kardar, Parisi, & Zhang, 1986). Other authors derive similar models (Ni & Christofides, 2005). As a first step, we will try some of these models, but we will also use a cellular automata model (Prieto-Langarica, Kojouharov, & Chen-Charpentier, 2013), to model the adsorption of molecules into the surface. This model also allows movement to reduce the total energy and has a random component. By using the scaling techniques presented in that paper, a new equation for the height of the surface can be developed. Stochastic partial differential equations need numerical methods to approximate their solutions. We will use stochastic Taylor expansion-based numerical schemes to solve the models for the surface thickness (Jentzen & Kloeden, 2009). In the case of chemical reactions between the deposited molecules and the substrate, it is necessary to add an attraction term to the above mentioned models. Once the surface is formed, the release of Si and its reaction with the near-surface boundary layer need to be modelled. The reaction rates need to be determined experimentally, but all chemical reactions, both fast and slow, globally or in steps, can be modelled using ordinary differential equations (Klipp, Liebermeister, Wierling, & Kowald, 2016).

For the reactions involving the use of ions with the superoxide dismutase equation, we assumed the presence of the cation on a free surface and acting as a catalyst for the reduction of superoxide to peroxide by SOD-1. The surface is described above. The mass action model incorporates the following reactions for conversion of superoxide to peroxide and the effect of Si^{4+} and Cu^{2+} as catalysts that promote the conversion of superoxide to peroxide via SOD reduction and charge transfer. Using the mass balance and mass action differential equations, the rate constant was determined to be approximately 0.0000020 $s^{-1,}$ assuming the reaction is first order.

The calculated results are presented as concentration as a function of reaction time. The reaction time that is input into the model covers the time of near-instantaneous addition of the experimental and control treatment groups to their long-term effect beyond the bone healing time period.

3 | RESULTS

3.1 | HUVECs viability exposed to different H_2O_2 concentrations

HUVECs were exposed to different concentrations of H_2O_2 to determine cell viability (at 6 and 24 hr). MTS proliferation assay showed that H_2O_2 0.2 and 0.4 mM presented no significant difference compared with control (EGM without H_2O_2). However, the number of viable cells was significantly increased compared with the other H_2O_2 groups ($p < 0.001$; Figure 1a). H_2O_2 0.6 mM was the first studied level to demonstrate a significant decrease compared with control ($p < 0.001$; Figure 1a). The other groups, $H_2O_2 > 0.6$ mM,

demonstrated to be highly toxic to HUVECs after 24 hr, with a significant decrease or absent viable cells number. H_2O_2 0.6 mM was considered and used for our experiment due to its capability of maintaining cell survival at a recoverable level, showing approximately 55% cell viability relative to initial cell seeding. Moreover, this concentration significantly reduced the viable HUVECs' number, as compared with control to 45 ± 21% ($p < 0.001$) and 64 ± 23% ($p < 0.001$) after 6 and 24 hr, respectively (Figure 1a). The Calcein-AM fluorescent images corroborate the MTS assay results, showing the reduction of viable cells at 6 and 24 hr (Figure 1b).

3.2 | Silicon ion effect on HUVECs under normal condition

3.2 1 | Cell viability—The effect of the silicon ion on the HUVECs' viability was tested under normal conditions. The silicon ion had no cytotoxic effect on any concentrations used in this experiment; all groups presented an increase in cell number compared with the initial cell seeding. However, after 6 hr, the cells exposed to Si^{4+} 1.0 mM presented no significant increase. At 24 hr, Si^{4+} 0.5 mM presented a significant increase in the relative cell number (3.21 ± 0.05-fold, $p < 0.05$) compared with the 0.1-, 1.0-mM silicon concentrations, and negative control (EBM).The positive control (EGM) showed the most significant increase in viable cells number (3.95 ± 0.07-fold, $p < 0.05$; Figure 1a).

3.2.2 | Cell proliferation—Cell proliferation was tested at 6 and 24 hr. After 6 hr, the groups with silicon ion presented similarly to the twofold more cells than control groups ($p < 0.05$). At 24 hr, the positive control (EGM) presented a significant increase (4.6 ± 0.22-fold; $p < 0.05$) among all groups. Finally, 48 hr after initial cell seeding, the positive control (EGM) had the most significant cell growth (8.04 ± 0.42-fold, $p < 0.01$). Nevertheless, among the silicon ion groups, the Si^{4+} 0.5 mM presented a significant increase of cell growth (4.39 ± 0.28-fold, $p < 0.05$) compared with the Si^{4+} 0.1 mM (3.44 ± 0.25-fold) and Si^{4+} 1.0 mM (3.12 ± 0.34-fold) groups (Figure 2b).

After 48 hr, the viable cell counting relative to positive control (EGM) showed that the 0.5-mM Si^{4+} group presented twofold more than the other silicon ion groups ($p < 0.05$) and fivefold greater than the negative control (EGM 20%, $p < 0.01$; Figure 2c and 2d).

3.3 | Capillary tube formation

3.3.1 | HUVECs seeded on bed of Matrigel—Capillary tube formation of HUVECs was tested on a bed of Matrigel exposed to different silicon ion concentrations: EGM (positive control) and EBM (negative control) specific environment. Si^{4+} 0.5 mM samples showed a significant enhancement of capillary tube formation among all groups, especially on the number of meshes ($p < 0.01$), which is closely related with precapillary structure maturity (Figure 3a and 3b).

3.3.2 | HUVECS seeded without Matrigel—All silicon ion groups presented a morphological cell shape change with the cells tending to form a capillary precursor structure (circular structures labelled in Figure 3c). All silicon groups formed significantly greater number of connected networks, at least 10-fold more than control (EBM). The 0.5-

mM Si^{4+} group formed 10-fold more connected networks than the 0.1-mM Si^{4+} ($p < 0.05$) and 20-fold more than the 1.0-mM Si^{4+} group ($p < 0.01$; Figure 3d).

3.4 | Scratch wound healing assay

A wound healing assay was used to test the amount of cell migration on a scratched surface. After fixation and staining with Toluidine blue, the bright field pictures (5× view) show the greatest amount of cell migration across the scratched area of the positive control group (EGM), followed by EBM + 0.5-mM Si^{4+} (Figure 4a). After measurements using Wound Healing (ImageJ plug-in), the data analysis showed that the addition of 0.5-mM Si^{4+} to EBM increased the HUVEC migration almost threefold on the scratched area after 12 hr (Figure 4b).

3.5 | Transwell migration assay

After fixation of the HUVECs, DAPI staining, and image capturing in 10×, 20×, and 40× (Figure 4c), the number of migrated cells was calculated. The data show that the silicon treatment group presented approximately twofold increase in migrated cell numbers, as compared with the negative control (EBM + 2% FBS, $p < 0.05$; Figure 4c and 4d).

3.6 | Effect of silicon ion on HUVECs under harmful hydrogen peroxide level

3.6.1 | Cell viability—After 6 and 24 hr, the silicon treatment group presented a significant increase in the live cells number, as compared with the nontreatment group ($p < 0.05$; Figure 5a and 5b). After 24 hr, HUVECs exposed to harmful levels of hydrogen peroxide (H_2O_2 0.6 mM), and silicon ion 0.5 mM simultaneously presented almost threefold decrease in dead cell numbers, as compared with cells exposed to hydrogen peroxide without silicon treatment ($p < 0.05$; Figure 5c and 5d).

3.6.2 | Quantitative real-time polymerase chain reaction—After 24 hr of cell seeding, the cell lysate was collected and analysed. All groups were compared with control EBM 20% and expressed relative to the housekeeping genes 18S and GAPDH. Cells exposed to 0.6-mM H_2O_2 presented a significant decrease of studied angiogenic genes expression, as compared with the control ($p < 0.01$). Cells exposed to the silicon ion presented a significant increase in the expression of all angiogenic genes studied ($p < 0.001$). The difference was more evident when compared with the 18S housekeeping gene: VEGF (7.13 ± 0.54-fold, $p < 0.01$), KDR (4.92 ± 1.18-fold, $p < 0.01$), and HIF-1α (5.97 ± 2-fold, $p < 0.01$; Figure 6a). Similarly, but with less intensity, all genes were significantly overexpressed relative to GAPDH: VEGF (5.3 ± 1-fold, $p < 0.05$), KDR (4 ± 0.73-fold, $p < 0.05$) and HIF-1α (3 ± 0.86-fold, $p < 0.05$; Figure 6b).

The results show that cells exposed to 0.6-mM H_2O_2 and treated with 0.5-mM Si^{4+} presented a significant overexpression as compared with the control, and relative to the 18S housekeeping gene: VEGFA (3.49 ± 0.75-fold, $p < 0.01$), KDR (2.38 ± 0.58-fold), and HIF-1α (2.77 ± 0.45-fold; Figure 6a). When GAPDH was considered as the housekeeping gene, there was a significant overexpression of VEGFA (4.36 ± 0.68-fold, $p < 0.001$) and HIF-1α (1.73 ± 0.42-fold, $p < 0.05$; Figure 6b).

Lastly, we tested the effect of ionic silicon (0.5 mM) in SOD-1, Cat-1, and NOS3 gene expression in HUVECs, under normal and toxic oxidative stress condition induced by H_2O_2 (0.6 mM). The 18S was used as housekeeping gene, and the results were compared with control and shown in Figure 6c–e. The Si^{4+} group showed a significant increase in mRNA levels of SOD-1 ($p = 0.001737$), Cat-1 ($p = 0.001046$), and NOS3 ($p = 0.000175$). The H_2O_2 group showed a significant reduction of NOS3 gene expression ($p = 0.0015191$). And H_2O_2 + Si^{4+} group also demonstrated an enhancement in mRNA levels of SOD-1 (0.02651), Cat-1 ($p = 0.01862$), and NOS3 ($p = 0.000178$).

3.7 | Computational model of ionic silicon and amorphous silica-based implants effect in superoxide dismutase cellular expression and ROS reduction

Silicon oxynitride coatings were fabricated using PECVD as described in Section 2 and detailed in previous publications (Ilyas et al., 2015; Ilyas et al., 2016). The coated materials were fabricated onto both the cylindrical and planar substrates, prior to in vitro cell-free studies. Cylindrical surgical stainless-steel rods were coated to examine coating uniformity and element homogeneity, as was observed in Figure 7. Planar substrates (Figure 8a) were used for determining the film thickness versus immersion time (Figure 8b). The overall coating thickness was nearly 1,000 nm prior to immersion testing. Cell free in vitro testing showed that the film thickness decreased as a function of the immersion time (Figure 8b). Because the samples are composed only of amorphous Si, O, and N, they will release ionic Si as a cation into the in vitro environment. We converted the film thickness change to the estimated rate of ionic Si release, based on the density of the film and molecular weight of silanol, converting this into the moles of ionic Si released (Figure 8c). It can be seen that the release of ionic Si was linear with immersion time. After this time, the surface was analysed for the formation of possible hydroxyapatite crystallites (Figure 8d). We confirmed the presence of these crystals, which resembled nano-hydroxyapatite (nano-HA) crystals, as was observed in our previous work (Ilyas et al., 2016).

The effect of SiON surfaces and ionic Si release on SOD-1 expression was also tested. It was found that the SiON ($n = 1.82$) surfaces as well as SiO ($n = 1.45$) and SiN ($n = 2.00$) surfaces induced a 2- to 2.5-fold increase in SOD-1 gene expression (Figure 9a,b) and ROS was reduced by nearly 30% (from a starting concentration of 0.015 μM) with increasing Si dose (Figure 9c). Meanwhile, there was a threefold SOD-1 overexpression with increasing ionic Si dose. Moreover, human porcine endothelial cells were found to have a higher density and with more elongated shape on the $SiON_x$ surfaces (Figure 9d), as compared with uncoated surfaces (Figure 9e).

To model these reactions to reduce ROS using ionic Si, we employed a mass action model that compared the effect of ionic Si treatment versus control (Cu^{2+}) cation. The model was a mass action model, and the equations used therein are given in Table 2. The time of study was at near instantaneous (time < 0.01 hr) to the long-term effect after the bone should be fully regenerated (time-10,000 hr). The concentration of ROS was initially set to approximately 80 ppm of superoxide. Our model shows that the addition of ionic silicon reduces the time period for the reaction to reach an equilibrium point, at which each mole of

superoxide is converted into a mole of peroxide. This enhancement was nearly fourfold (8 hr) for the ionic Si treatment, as compared with the control treatment (32 hr; Figure 10a,b).

4 | DISCUSSION

Our study shows the novel effect of the ionic silicon on HUVECs under harmful oxidative stress. There was significant enhancement on cell viability and reduction of cell death on HUVECs exposed to H_2O_2 0.6 mM in the presence of Si^{4+} 0.5 mM. Furthermore, the same condition exhibited an enhancement on expression of VEGFA, VEGFR-2, and HIF-1α, which are major angiogenic markers. In addition, there was an overexpression of antioxidant enzymes SOD-1 and Cat-1, and NOS3 that maybe contributed for a protective effect on studied cells under toxic oxidative stress environment.

The concentration of 0.6-mM hydrogen peroxide was selected for these experiments due to its significant reduction of HUVEC viability. The chosen concentration also allowed some degree of cell survival, which could be enough for cell recovery by the positive effect of the silicon ion. Other studies have used this same concept (Wen et al., 2013), but we verified the conditions for our designed experiment because, as mentioned in the material section, we have used a unique combination of cells and growth media. Superoxide is the main ROS produced in hypoxic conditions. Nevertheless, it is highly unstable and gets converted to hydrogen peroxide (Kim & Byzova, 2014). Hence, hydrogen peroxide has been used in a variety of studies (Csordas, Wick, & Bernhard, 2006; Song, Pu, & He, 2014; Wei, Li, Hu, Chen, & Cong, 2010; Wen et al., 2013).

Oxidative stress is a condition present at the beginning of bone regeneration after trauma and can lead to a deleterious effect on osteoblasts and endothelial cells, impairing new bone and vascular structure and formation (Arai, Shibata, Pugdee, Abiko, & Ogata, 2007; Prasad, Dhillon, Khullar, & Nagi, 2003; Yeler, Tahtabas, & Candan, 2005). In vivo models are unable to precisely identify the reactive species levels and toxicity due to its molecular instability. Therefore, ROS' production has been specifically studied in vitro. Some studies used hypoxic chamber (Yang et al., 2014; Zhang et al., 2016), but hydrogen peroxide appears to more realistically mimic the oxidative stress in an acute bone loss situation. The concentration of H_2O_2 is controversial, depending on a variety of factors, such as condition media, cell type, and passage. In our study, we used H_2O_2 0.6 mM; similar studies have been designed with other concentrations due to usage of different condition media and cells (Csordas et al., 2006; Wei et al., 2010; Wen et al., 2013).

Our study investigated the effect of three silicon ion concentrations (0.1, 0.5, and 1.0 mM) on the HUVECs' viability and proliferation under normal conditions (nonpro-oxidant or no H_2O_2). The experimental silicon concentrations were non-toxic to the HUVECs at the concentrations tested. Thus, 0.5-mM Si^{4+} showed an increase in cell proliferation after 48 hr, potentially being a therapeutic dosage for use in unfavourable situations, such as after a trauma or injury, to combat the harmful hydrogen peroxide concentrations observed in these hypoxic environments. Contrary to our observation, a study using the same silicon ion groups showed no effect on the HUVEC's proliferation under normal conditions (Robertson, 2009). We believe that the difference observed in our experiment was due to specific

changes and reductions in the growth factor used in the cell culture media of silicon ion groups, allowing the cells to be exposed to an in vitro environment with enough nutrition to demonstrate a potentially beneficial effect of the silicon ion on cell proliferation and without significant added effect from growth factors. The enhancement on cell proliferation can be associated with VEGFR-2 and VEGFA upregulation, such as was described previously (Koch, Tugues, Li, Gualandi, & Claesson-Welsh, 2011), and observed in the gene expression of the present study (Figure 6).

All silicon ion concentrations used in this study induced marked morphological change, forming enhanced capillary-like structure on the HUVECs cultured in normal condition without Matrigel (Figure 3c and 3d). This observation needs further investigation to better understand silicon's effect on the cytoskeleton and cell-to-cell interaction. The tube formation on the bed of Matrigel showed the enhancement of capillary-like tube formation precursors in the presence of 0.5-mM Si^{4+}, particularly demonstrated by the increased number of matured structures and mesh networks (Figure 3a and 3b). Some studies, which evaluated materials based on silicon, also presented a similar result; however, the effect was verified in combination with other elements, such as calcium and magnesium (Dashnyam et al., 2017; Kong, Lin, Li, & Chang, 2014). Endothelium cells' capillary tube formation is correlated with a cascade downstream of integrin ligation induced by cell matrix interaction (Davis & Senger, 2005; Davis, Kon, & Stratman, 2007). Nesprins are proteins that link the cell nuclei to the cytoskeleton and are associated with the HUVECs' loop formation during angiogenesis (King et al., 2014). We speculate that Si^{4+} can have some effect on the cell matrix interaction and/or nesprin activation and expression, and further investigation is necessary for clarification.

The presence of ionic silicon increased the capillary tube formation structure, with and without Matrigel. At the same time point, the three silicon groups demonstrated an enhancement of twofold on the cell proliferation compared with the controls (Figure 2b–d). However, capillary tube formation assay with Matrigel cannot be correlated with the first 6 hr' proliferation results (Figure 2b), because the cell culture condition of Matrigel is rich in endothelial cells' growth factor, and proteins are not present in the cell culture media used in the proliferation study. The same must be considered in the tube formation experiment without Matrigel, when a marked increase in the capillary-like tube structure was observed in groups with silicon and minimum cell culture condition on EBM (without growth factors; Figure 3c and 3d).

The present study showed that 0.5-mM Si^{4+} significantly increased cell migration in the scratch assay (Figure 4a and 4b) and had a chemotactic effect on HUVECs, confirmed by the transwell cell migration, which showed significant improvement as compared with the negative control (EBM; Figure 4c and 4d). Cell migration is a relevant phenomenon during angiogenesis, and its enhancement would greatly impact the tissue healing process. The transwell cell migration simulated the effect of silicon ions released by the biomaterials used in bone tissue replacement and/or stabilizer. Both results were reinforced by a current publication that used mesoporous silica (Dashnyam et al., 2017).

The present study demonstrates that HUVECs exposed to H_2O_2 0.6 mM (toxic levels) and treated with Si^{4+} 0.5 mM reduces cell death and enhancement of cell survival on live/dead cell fluorescent staining (Figure 5). These findings suggest that the silicon ion can limit cell death during the first 24 hr, on cells exposed to unfavourable oxidative stress present in injuries and bone loss. Recently, a few studies have been focused on effects of biomaterials/implants used on oxidative stress induced by bone defects (Ilyas et al., 2016; Sansone, Pagani, & Melato, 2013). These studies have focused on the long-term outcome of oxidative stress and its association with implant loosening and failure (Kinov et al., 2006; Pietropaoli et al., 2013; Sansone et al., 2013). Yet these studies neglected research on early time points, as the period is crucial for angiogenesis and efficient tissue repair for improved long-term implant or biomaterial attachment and potentially reduce failure rates.

The studied angiogenic genes expressed a consistent pattern with significant overexpression under harmful oxidative stress when treated with the silicon ion (Figure 6), reinforcing the observation of live/dead HUVEC microscopy and MTS proliferation assays (Figure 5). Studies correlate silicon-based materials with a positive effect on angiogenesis and enhanced expression of VEGF and VEGFR-2 in HUVECs in vitro (Li & Chang, 2013; Zhai et al., 2012). Nevertheless, none of these studies showed the effect of ionic silicon in HUVECs angiogenesis in the real clinical situation of unfavourable oxidative stress.

Our study showed underexpression of VEGFA, VEGFR-2, and HIF-1α in HUVECs exposed to a harmful hydrogen peroxide concentration and recovery, with overexpression in silicon treatment groups. HIF-1α overexpression in a treatment group corroborates the fact that HUVECs have a higher survival rate and less cell death under harmful H_2O_2 concentrations. HIF-1α activation is a master event in the downstream signalling of angiogenesis (Krock, Skuli, & Simon, 2011). HIF-1α is necessary for blood vessel invasion and progenitor cell survival in hypoxic and damaged environments, especially when the blood vessels have not reached the site of injury. Downstream in the pathway, HIF-1α reduces oxygen consumption to help avoid harmful ROS accumulation (Stegen et al., 2016). HIF-1α proved to be essential for new bone formation on the osteoblast progenitor cells by upregulating the angiogenic markers (Stegen et al., 2016). A recent publication showed a relationship between the silicon ion released from mesoporous microcarriers and HIF1-α upregulation by HUVECs under regular cell culture media conditions without toxic levels of ROS (Dashnyam et al., 2017). Our results corroborated these findings and showed increased HIF-1α expressed in HUVECs exposed to harmful levels of hydrogen peroxide.

The present study shows that VEGFA expression is significantly increased in HUVECs exposed to 0.5-mM Si^{4+}, even when the cells were under harmful oxidative stress. The VEGFR-2 followed the same pattern but with less increase. VEGFA and analogous receptor (VEGFR-2) are crucial in both angiogenesis and regulation of long-term blood vessel formation (Hu & Olsen, 2016). Moreover, VEGFA and VEGFR-2 play a significant role in the different stages of endochondral and intramembranous ossification, having a paracrine, autocrine, and intracrine effect on osteoblast function during the bone repair (Hu & Olsen, 2016). Hence, our results support the beneficial effect of Si^{4+} under normal and deleterious levels of H_2O_2, showing overexpression of the relevant genes related with new blood vessel formation.

Antioxidant enzymes play a relevant role in the reduction of oxidative stress. SOD-1 participate in conversion of superoxide into peroxide, for further conversion of hydrogen peroxide into water and oxygen by Cat-1. These mechanisms contribute to the equilibrium of oxidative stress. There are some enzymes and molecules that contribute to the equilibrium of pro-oxidant and antioxidant systems. However, SOD-1, Cat-1, and NOS3 were considered in our study, due to their close correlation with angiogenesis and osteogenesis (Choi et al., 2012; Fernández et al., 2009; Gabryel et al., 2016; Ilyas et al., 2016). Moreover, the SOD-1 demonstrated a protective effect in HUVECs under oxidative stress and oxygen deprivation, reducing apoptosis of endothelial cells (Gabryel et al., 2016). In the present publication, we showed that the SOD-1 mRNA levels were elevated in HUVECs exposed to 0.5-mM Si^{4+} under normal and oxidative stress conditions that corroborate preosteoblast findings referred to by our group in a previous publication (Ilyas et al., 2016). Perhaps, these findings justify a reduction in HUVECs death verified in the live and dead assay results of the present study. In addition, the reduction of oxidative stress and less toxic environment could be demonstrated by overexpression of Cat-1. The NOS3 is an enzyme mostly produced by endothelial cells, and its function is to produce nitric oxide (NO), which plays a significant role in tissue adequate perfusion. Further, studies have demonstrated that NOS3 can be important for cell mobilization on angiogenesis and tissue regeneration (Aicher et al., 2003). Our results showed a significant enhancement in HUVECs NOS3 expression in ionic silicon group under normal and toxic oxidative stress conditions (Figure 6e) that can be favourable for the functioning and viability of endothelial cells.

The effect that Si^{4+} plays on angiogenesis was probably analogous to our previous work in osteogenesis. In that work (Ilyas et al., 2016), it was found that osteogenic transcription was dependent on ionic Si enhancement of SOD-1. Probably a similar link could have occurred for angiogenesis. For example, elevated superoxide dismutase activity (sixfold) under hypoxic conditions (<4% O_2) led to HIF-1α stabilization and new blood vessel formation (Movafagh, Crook, & Vo, 2015; M. Wang et al., 2005). Other studies have noted a reduction of ROS and its products by other antioxidants such as glutathione family of antioxidants (e.g., glutathione [GSH], glutathione peroxidase [GPX1]; Armstrong et al., 2002; Marí, Morales, Colell, García-Ruiz, & Fernández-Checa, 2009). For example, the glutathione family of antioxidants has been linked to have a stimulatory effect on HIF-1α and VEGFA under conditions of oxidative stress (Galasso et al., 2006; Marí et al., 2009). The study demonstrated inhibition or limitation of new blood formation in mice deficient of GPX1 (Galasso et al., 2006). It may be possible that ionic Si enhances angiogenic markers as seen in the present work by the improvement of antioxidant enzymes expressions. Future work will explore these important mechanisms because they play an essential role in mitigating deleterious oxidative stress and promoting angiogenesis and bone healing. Further investigation is necessary for understanding the angiogenic and antioxidant effect of silica-based materials used for bone replacement and support in in vitro and in vivo experiments.

In the last section of this manuscript, we described a computational model that demonstrated the possible effect of ionic silicon on reduction of oxidative stress during angiogenesis and osteogenesis. This reduction in ROS within a few hours after treatment to equilibrium is an important marker of the effectiveness of ionic Silicon to reduce ROS. Moreover, this is an indication of the impact of valence states of ions in redox reactions. The added results of our

ability to coat current implants used to regenerate both bone and vasculature and sustain the release of these ions over several weeks give added impact to the potential of the materials to continuously mitigate the prolonged and harmful effects of oxidative stress, while in turn stimulating endothelial cell activity.

5 | CONCLUSION

This study demonstrates that ionic silicon markedly enhances HUVEC viability, even in unfavourable conditions of harmful levels of ROS (H_2O_2). The silicon ion also induces a significant morphological change, with or without the favourable Matrigel condition, forming capillary precursor tube structures. Our results also show the enhancement on cells' migration in a wounded area (scratch assay) and by homing effect (transwell migration). These findings strongly support the idea that the controlled release of silicon ion by biomaterials used in bone tissue engineering can have a beneficial effect in the early stages of tissue regeneration by enhancing new blood vessel formation, a crucial step in the healing process. We believe that future studies need to focus on understanding how the silicon ion induces HUVEC cytoskeleton changes, and the specific mechanism responsible by beneficial silicon ion effect on HUVECs' survival under harmful, oxidative stress.

ACKNOWLEDGEMENTS

The authors would like to thank Olumide Aruwajoye, Suresh Adapala, lla Oxendine, Yang Li, Reuel Cornelia, and Richard Banlaygas from the Center for Excellence in Hip Disorders, Texas Scottish Rite Hospital, for their assistance. We would like to thank the Brazilian Federal Government—Coordenacao de Aperfeicoamento de Pessoal de Nivel Superior (CAPES), for sponsoring the first author.

This work was supported by a grant from the National Institutes of Health (1R03DE023872-01A1) to V. G. Varanasi.

Funding information

Enhancement Grant, Grant/Award Number: 24444100005; Departmental Startup, Grant/Award Number: 304-128170; National Institutes of Health, Grant/Award Number: 1R03DE023872-01A1

REFERENCES

Arai M, Shibata Y, Pugdee K, Abiko Y, & Ogata Y (2007). Effects of reactive oxygen species (ROS) on antioxidant system and osteoblastic differentiation in MC3T3-E1 cells. IUBMB Life, 59, 27–33. [PubMed: 17365177]

Armstrong JS, Steinauer KK, Hornung B, Irish JM, Lecane P, Birrell GW Knox SJ (2002). Role of glutathione depletion and reactive oxygen species generation in apoptotic signaling in a human B lymphoma cell line. Cell Death and Differentiation, 9, 252–263. [PubMed: 11859408]

Arnaoutova I, & Kleinman HK (2010). In vitro angiogenesis: Endothelial cell tube formation on gelled basement membrane extract. Nature Protocols, 5, 628–635. [PubMed: 20224563]

Asselin A, Hattar S, Oboeuf M, Greenspan D, Berdal A, & Sautier JM (2004). The modulation of tissue-specific gene expression in rat nasal chondrocyte cultures by bioactive glasses. Biomaterials, 25, 5621–5630. [PubMed: 15159078]

Chen G, Zhao L, Feng J, You G, Sun Q, Li P, … Zhou H (2013). Validation of reliable reference genes for real-time PCR in human umbilical vein endothelial cells on substrates with different stiffness. PLoS One, 8, e67360. [PubMed: 23840676]

Csordas A, Wick G, & Bernhard D (2006). Hydrogen peroxide-mediated necrosis induction in HUVECs is associated with an atypical pattern of caspase-3 cleavage. Experimental Cell Research, 312, 1753–1764. [PubMed: 16530181]

Dashnyam K, Jin G, Kim J, Perez R, Jang J, & Kim H (2017). Promoting angiogenesis with mesoporous microcarriers through a synergistic action of delivered silicon ion and VEGF. Biomaterials, 116, 145–157. [PubMed: 27918936]

Davis GE, Kon W, & Stratman AN (2007). Mechanisms controlling human endothelial lumen formation and tube assembly in three-dimensional extracellular matrices. Birth Defects Research Part C - Embryo Today: Reviews, 81, 270–285.

Davis GE, & Senger DR (2005). Endothelial extracellular matrix: Biosynthesis, remodeling, and functions during vascular morphogenesis and neovessel stabilization. Circulation Research, 97, 1093–1107. [PubMed: 16306453]

Galasso G, Schiekofer S, Sato K, Shibata R, Handy DE, Ouchi N, … Walsh K (2006). Impaired angiogenesis in glutathione peroxidase-1-deficient mice is associated with endothelial progenitor cell dysfunction. Circulation Research, 98, 254–261. [PubMed: 16373599]

Hench LL, Splinter RJ, Allen WC, & Greenlee TK (1971). Bonding mechanisms at the interface of ceramic prosthetic materials. Journal of Biomedical Materials Research, 5, 117–141.

Hu K, & Olsen BR (2016). The roles of vascular endothelial growth factor in bone repair and regeneration. Bone, 91, 30–38. [PubMed: 27353702]

Ilyas A, Lavrik NV, Kim HKW, Aswath PB, & Varanasi VG (2015). Enhanced interfacial adhesion and osteogenesis for rapid “bone-like” biomineralization by PECVD-based silicon oxynitride overlays. ACS Applied Materials & Interfaces, 7, 15368–15379. [PubMed: 26095187]

Ilyas A, Odatsu T, Shah A, Monte F, Kim HKW, Kramer P, … Varanasi VG (2016). Amorphous silica: A new antioxidant role for rapid critical-sized bone defect healing. Advanced Healthcare Materials, 5, 2199–2213. [PubMed: 27385056]

Kim Y, & Byzova TV (2014). Oxidative stress in angiogenesis and vascular disease. Blood, 123, 625–631. [PubMed: 24300855]

King SJ, Nowak K, Suryavanshi N, Holt I, Shanahan CM, & Ridley AJ (2014). Nesprin-1 and nesprin-2 regulate endothelial cell shape and migration. Cytoskeleton, 71, 423–434. [PubMed: 24931616]

Kinov P, Leithner A, Radl R, Bodo K, Khoschsorur G, Schauenstein K, & Windhager R (2006). Role of free radicals in aseptic loosening of hip arthroplasty. Journal of Orthopaedic Research, 24, 55–62. [PubMed: 16419969]

Koch S, Tugues S, Li X, Gualandi L, & Claesson-Welsh L (2011). Signal transduction by vascular endothelial growth factor receptors. The Biochemical Journal, 437, 169–183. [PubMed: 21711246]

Kong N, Lin K, Li H, & Chang J (2014). Synergy effects of copper and silicon ions on stimulation of vascularization by copper-doped calcium silicate. Journal of Materials Chemistry B, 2, 1100.

Krock BL, Skuli N, & Simon MC (2011). Hypoxia-induced angiogenesis: Good and evil. Genes & Cancer, 2, 1117–1133. [PubMed: 22866203]

Li H, & Chang J (2013). Bioactive silicate materials stimulate angiogenesis in fibroblast and endothelial cell co-culture system through paracrine effect. Acta Biomaterialia, 9, 6981–6991. [PubMed: 23416471]

Lu C, Marcucio R, & Miclau T (2006). Assessing angiogenesis during fracture healing. The Iowa Orthopaedic Journal, 26, 17–26. [PubMed: 16789443]

Marí M, Morales A, Colell A, García-Ruiz C, & Fernández-Checa JC (2009). Mitochondrial Glutathione, a key survival antioxidant. Antioxidants & Redox Signaling, 11, 2685–2700. [PubMed: 19558212]

Morin KT, & Tranquillo RT (2013). In vitro models of angiogenesis and vasculogenesis in fibrin gel. Experimental Cell Research, 319, 2409–2417. [PubMed: 23800466]

Movafagh S, Crook S, & Vo K (2015). Regulation of hypoxia-inducible factor-1a by reactive oxygen species: New developments in an old debate. Journal of Cellular Biochemistry, 116, 696–703. [PubMed: 25546605]

Odatsu T, Azimaie T, Velten MF, Vu M, Lyles MB, Kim HK, … Varanasi VG (2015). Human periosteum cell osteogenic differentiation enhanced by ionic silicon release from porous amorphous silica fibrous scaffolds. Journal of Biomedical Materials Research. Part A, 103, 2797–2806. [PubMed: 25630903]

Pietropaoli D, Ortu E, Severino M, Ciarrocchi I, Gatto R, & Monaco A (2013). Glycation and oxidative stress in the failure of dental implants: A case series. BMC Research Notes, 6, 296. [PubMed: 23890159]

Prasad G, Dhillon MS, Khullar M, & Nagi ON (2003). Evaluation of oxidative stress after fractures. A preliminary study. Acta Orthopaedica Belgica, 69, 546–551. [PubMed: 14748113]

Rasband WS (1997-2017), ImageJ, U. S. National Institute of Helath, Bethasda, Maryland, USA, https://imagej.nih.gov/ij/

Renno ACM, Bossini PS, Crovace MC, Rodrigues ACM, Zanotto ED, & Parizotto NA (2013). Characterization and in vivo biological performance of biosilicate. BioMed Research International, 2013, 1–7.

Robertson Z (2009), An in vitro study of the effect of silicon and magnesium ions on bone repair and angiogenesis, http://ethos.bl.uk/OrderDetails.do?uin=uk.bl.ethos.499725.

Ryter SW, Kim HP, Hoetzel A, Park JW, Nakahira K, Wang X, & Choi AMK (2007). Mechanisms of cell death in oxidative stress. Antioxidants & Redox Signaling, 9, 49–89. [PubMed: 17115887]

Saghiri MA, Asatourian A, Orangi J, Sorenson CM, & Sheibani N (2015). Functional role of inorganic trace elements in angiogenesis (Part I: N, Fe, Se, P, Au, and Ca). Critical Reviews in OncologyHematology, 96, 129–142.

Sansone V, Pagani D, & Melato M (2013). The effects on bone cells of metal ions released from orthopaedic implants. A review. Clinical cases in mineral and bone metabolism: the official journal of the Italian Society of Osteoporosis, Mineral Metabolism, and Skeletal Diseases, 10, 34–40.

Sharma P, Jha AB, Dubey RS, & Pessarakli M (2012). Reactive oxygen species, oxidative damage, and antioxidative defense mechanism in plants under stressful conditions. Journal of Botany, 2012, 1–26.

Sivaraman B, Swaminathan G, Moore L, Fox J, Seshadri D, Dahal S Ramamurthi A (2017). Magnetically-responsive, multifunctional drug delivery nanoparticles for elastic matrix regenerative repair. Acta Biomaterialia, 52, 171–186. [PubMed: 27884774]

Solaini G, Baracca A, Lenaz G, & Sgarbi G (2010). Hypoxia and mitochondrial oxidative metabolism. BBA - Bioenergetics, 1797, 1171–1177. [PubMed: 20153717]

Song W, Pu J, & He B (2014). Tanshinol protects human umbilical vein endothelial cells against hydrogen peroxide-induced apoptosis. Molecular Medicine Reports, 10, 2764–2770. [PubMed: 25189379]

Stegen S, Deprez S, Eelen G, Torrekens S, Van Looveren R, Goveia J, & GhesquiÃ¨re B, Carmeliet P, Carmeliet G (2016). Adequate hypoxia inducible factor la signaling is indispensable for bone regeneration. Bone, 87, 176–186. [PubMed: 27058876]

Tabak O, Gelisgen R, Erman H, Erdenen F, Muderrisoglu C, Aral H, & Uzun H (2011). Oxidative lipid, protein, and DNA damage as oxidative stress markers in vascular complications of diabetes mellitus. Clinical and Investigative Medicine. Medecine Clinique et Experimentale, 34, E163–E171. [PubMed: 21631993]

Technical Information. (2014), Clonetics â,,¢ Endothelial Cell System, 1–15.

Vacanti JP, & Langer R (1999). Tissue engineering: The design and fabrication of living replacement devices for surgical reconstruction and transplantation, 1: 32,33, 34.

Varanasi VG, Leong KK, Dominia LM, Jue SM, Loomer PM, &Marshall GW (2012). Si and Ca individually and combinatorially target enhanced MC3T3-E1 subclone 4 early osteogenic marker expression. The Journal of Oral Implantology, 38, 325–336. [PubMed: 22913306]

Wang D, Wang G, Liu M, Sun L, Zong W, Jiang H, … Sun S (2014). A novel animal model of osteonecrosis of the femoral head induced using a magnetic resonance imaging-guided argon-helium cryotherapy system. Experimental and Therapeutic Medicine, 7, 1525–1528. [PubMed: 24926337]

Wang M, Kirk JS, Venkataraman S, Domann FE, Zhang HJ, Schafer FQ, … Oberley LW (2005). Manganese superoxide dismutase suppresses hypoxic induction of hypoxia-inducible factor-1α and vascular endothelial growth factor. Oncogene, 24, 8154–8166. [PubMed: 16170370]

Wang X, Cheng F, Liu J, Smatt JH, Gepperth D, Lastusaari M, … Hupa L (2016). Biocomposites of copper-containing mesoporous bioactive glass and nanofibrillated cellulose: Biocompatibility and

angiogenic promotion in chronic wound healing application. Acta Biomaterialia, 46, 286–298. [PubMed: 27646503]

Wei H, Li Z, Hu S, Chen X, & Cong X (2010). Apoptosis of mesenchymal stem cells induced by hydrogen peroxide concerns both endoplasmic reticulum stress and mitochondrial death pathway through regulation of caspases, p38 and JNK. Journal of Cellular Biochemistry, 111, 967–978. [PubMed: 20665666]

Wen YD, Wang H, Kho SH, Rinkiko S, Sheng X, Shen HM, & Zhu YZ (2013). Hydrogen sulfide protects HUVECs against hydrogen peroxide induced mitochondrial dysfunction and oxidative stress. PLoS One, 8.

Yang L, Zheng J, Xu R, Zhang Y, Gu L, Dong J, … Du J (2014). Melatonin suppresses hypoxia-induced migration of HUVECs via inhibition of ERK/Rac1 activation. International Journal of Molecular Sciences, 15, 14102–14121. [PubMed: 25123138]

Yeler H, Tahtabas F, & Candan F (2005). Investigation of oxidative stress during fracture healing in the rats. Cell Biochemistry and Function, 23, 137–139. [PubMed: 15651080]

Zhai W, Lu H, Chen L, Lin X, Huang Y, Dai K, Naoki K, Chen G, & Chang J (2012), Silicate bioceramics induce angiogenesis during bone regeneration, 8: 341–349.

Zhang Q, Shang M, Zhang M, Wang Y, Chen Y, Wu Y, … Liu Y(2016). Microvesicles derived from hypoxia/reoxygenation-treated human umbilical vein endothelial cells promote apoptosis and oxidative stress in H9c2 cardiomyocytes. BMC Cell Biology, 17, 25. [PubMed: 27338159]

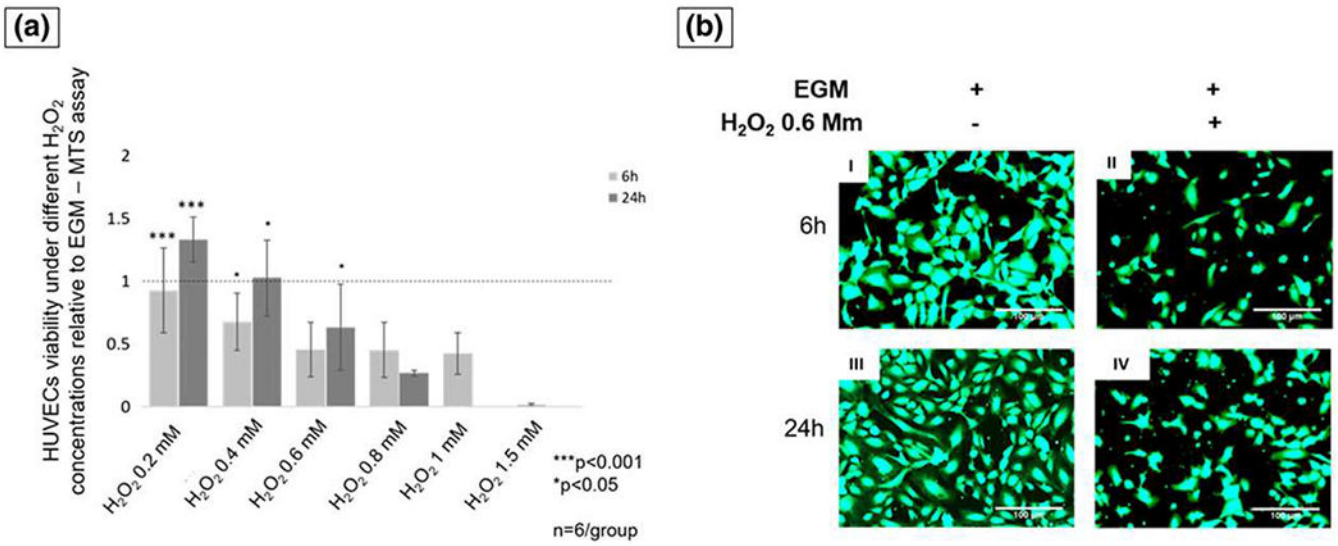

FIGURE 1.

(a) The cells number relative to control at 6- and 24-hr time points. At 24-hr, H_2O_2 0.6 mM was significantly lower than 0.4 mM and higher than 0.8 mM (ANOVA, $***p < 0.001$, $*p < 0.05$ indicate statistical significance, $n = 6$ per group). (b) Fluorescent pictures of human umbilical vein endothelial cells (HUVECs) stained with Calcein-AM at 6 hr (I and III) and 24 hr (II and IV). Pictures I and III show cells exposed to endothelial cell growth media (EGM), and pictures II and IV show cells exposed to EGM and hydrogen peroxide (H_2O_2; scale bar = 100 μm) [Colour figure can be viewed at wileyonlinelibrary.com]

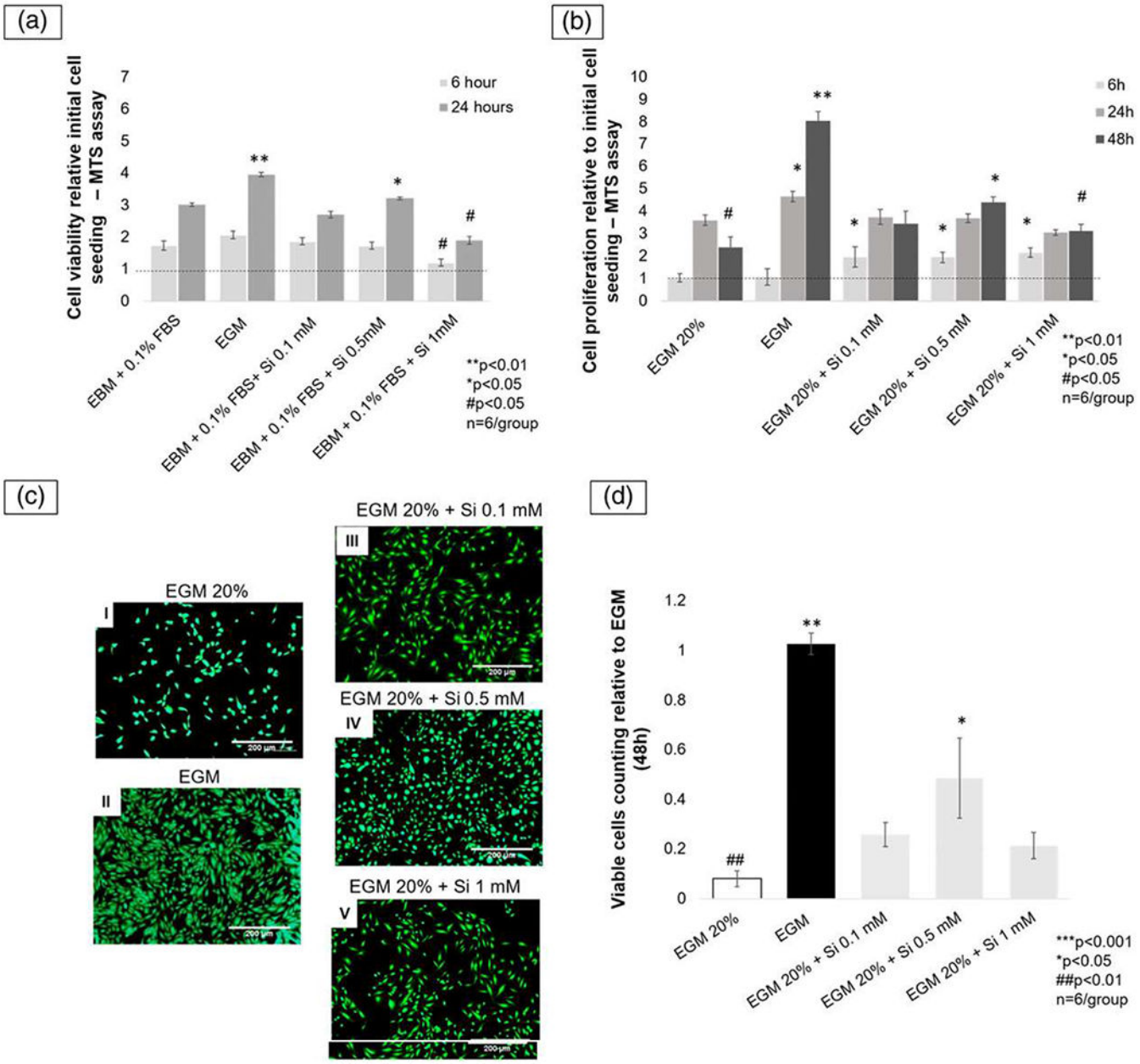

FIGURE 2.

(a) The bar graph shows the viable cells number measured by MTS assay after 6 and 24 hr. At 24 hr, Si^{4+} 0.5 mM presented the most significant among the silicon groups and EBM. $^{**}p < 0.01$, $^{*}p < 0.05$, $\#p < 0.05$; $n = 6$. (b) Bar graph shows cells proliferation relative to initial cell seeding after 6, 24, and 48 hr. At 6 hr, all silicon groups similarly presented a significant enhancement in relative cell growth, as compared with controls ($p < 0.05$). At 48 hr, among all silicon groups and EGM 20%, Si^{4+} 0.5 mM showed the most significant relative cell growth ($p < 0.05$). (c) Fluorescent pictures (5× view) of human umbilical vein endothelial cells (HUVECs) stained with Calcein-AM after 48 hr showed enhancement on cell proliferation after being exposed to ionic silicon. Picture I shows the reduced viable cells number on negative control (EGM 20%). Picture II shows an outstanding increase in

the cell numbers on positive control, followed by EGM 20% + Si^{4+} 0.5 mM group shown in picture IV. The other two silicon ion groups (pictures III and V) showed similar results with less viable cells than positive control and EBM 20% + Si^{4+} 0.5 mM (scale bar = 200 μm), (d) Bar graph showing viable cells number are relative to positive control (EGM). EGM 20% + Si^{4+} 0.5 mM group presented twofold more than the other silicon groups ($p < 0.05$) and fivefold more than negative control (EBM 20%; $p < 0.01$; ANOVA, ***$p < 0.001$, **$p < 0.01$, *$p < 0.05$, ##$p < 0.01$, #$p < 0.05$ indicate statistical significance; $n = 6$). EGM: endothelial cell growth media; EBM: endothelial cell basal media [Colour figure can be viewed at wileyonlinelibrary.com]

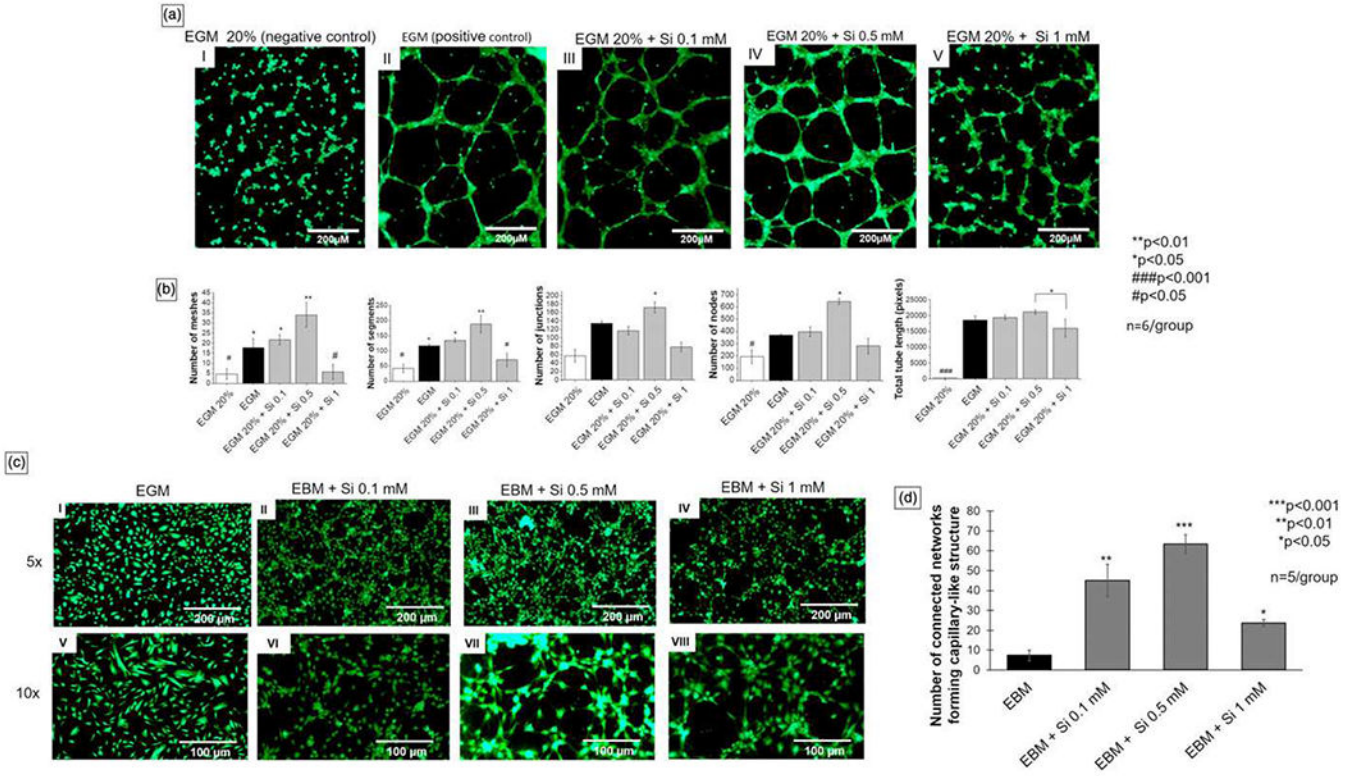

FIGURE 3.

(a) Pictures I, II, III, IV, and V show fluorescent pictures (5× view) of human umbilical vein endothelial cells (HUVECs) stained with Calcein-AM, 6 hr after seeding on bed of Matrigel. Si^{4+} 0.5 mM presented the best parameters among all groups, especially on the number of meshes and nodes (scale bar = 200 μm). (b) Analysis of data collected from ImageJ. Si^{4+} 0.5 mM presented significantly higher number of meshes, segments, junctions, and nodes when compared with other groups. (c) Fluorescent pictures of HUVECs stained with Calcein-AM, 3 hr after media change and 27 hr after initial cell seeding. Pictures I and V (control) show a low number of circles (5× view, scale bar = 200 μm). Pictures II, III, IV, VI, VII, and VIII represent the cells exposed to different silicon ion concentrations and show a higher number of circular structures, similar to precapillary tubes. (d) Bar graph showing the data analysis from the fluorescent pictures of number of connected networks formed according to group relative to control (EBM). EBM + Si^{4+} 0.5 mM produced the most remarkable results followed by 0.1 mM and 1 mM (10× view, scale bar = 100 μm; ANOVA, ***$p < 0.001$, **$p < 0.01$, *$p < 0.05$, ###$p < 0.001$, #$p < 0.05$ indicate statistical significance). EBM: endothelial cell basal media; EGM: endothelial cell growth media [Colour figure can be viewed at wileyonlinelibrary.com]

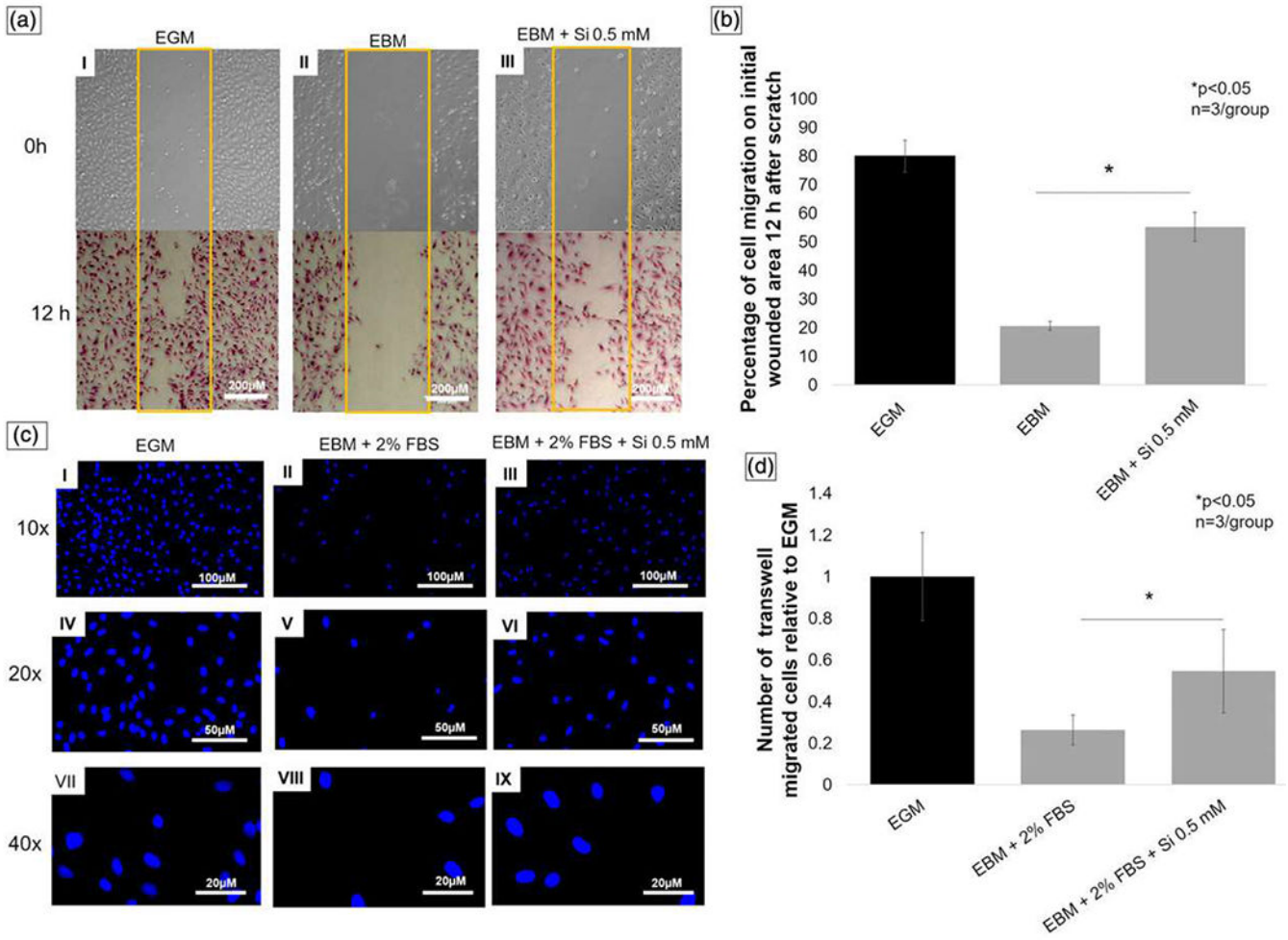

FIGURE 4.

(a) Scratch wound healing assay. Pictures (5× view) of wounded area on time 0 hr (no staining) and 12 hr (toluidine blue staining). Picture I shows EGM (positive control) group with higher wounded area occupied by migrated cells. Picture II shows EBM (negative control) group with lower number of cells on wounded area, and picture III represents EBM treated with Si^{4+} 0.5 mM showing the increase of silicon on cell migration, as compared with EBM (picture II; scale bar = 200 μm). (b) Graph shows percentage of occupied initial wounded area by migrated cells relative to control (EGM) 12 hr after scratch. EBM + Si^{4+} group presented almost three times more occupied area than EBM without silicon. (c) Fluorescent pictures of human umbilical vein endothelial cells stained with DAPI 12 hr after transwell cell migration. Pictures I, IV, and VII show EGM (positive control), pictures II, V, and VIII EBM + 2% FBS (negative control), and pictures III, VI, and IX silicon treatment group (10× view, scale bar = 100 μm; 20× view, scale bar = 50 μm; 40× view scale bar = 20 μm). (d) Bar graph presents number of transwell migrated cells relative to EGM (positive control). Silicon treatment group showed two times more cell migration than negative control (ANOVA, $*p < 0.05$ indicates statistical significance; $n = 3$ per group). EGM: endothelial cell growth media; EBM: endothelial cell basal media. FBS: fetal bovine serum [Colour figure can be viewed at wileyonlinelibrary.com]

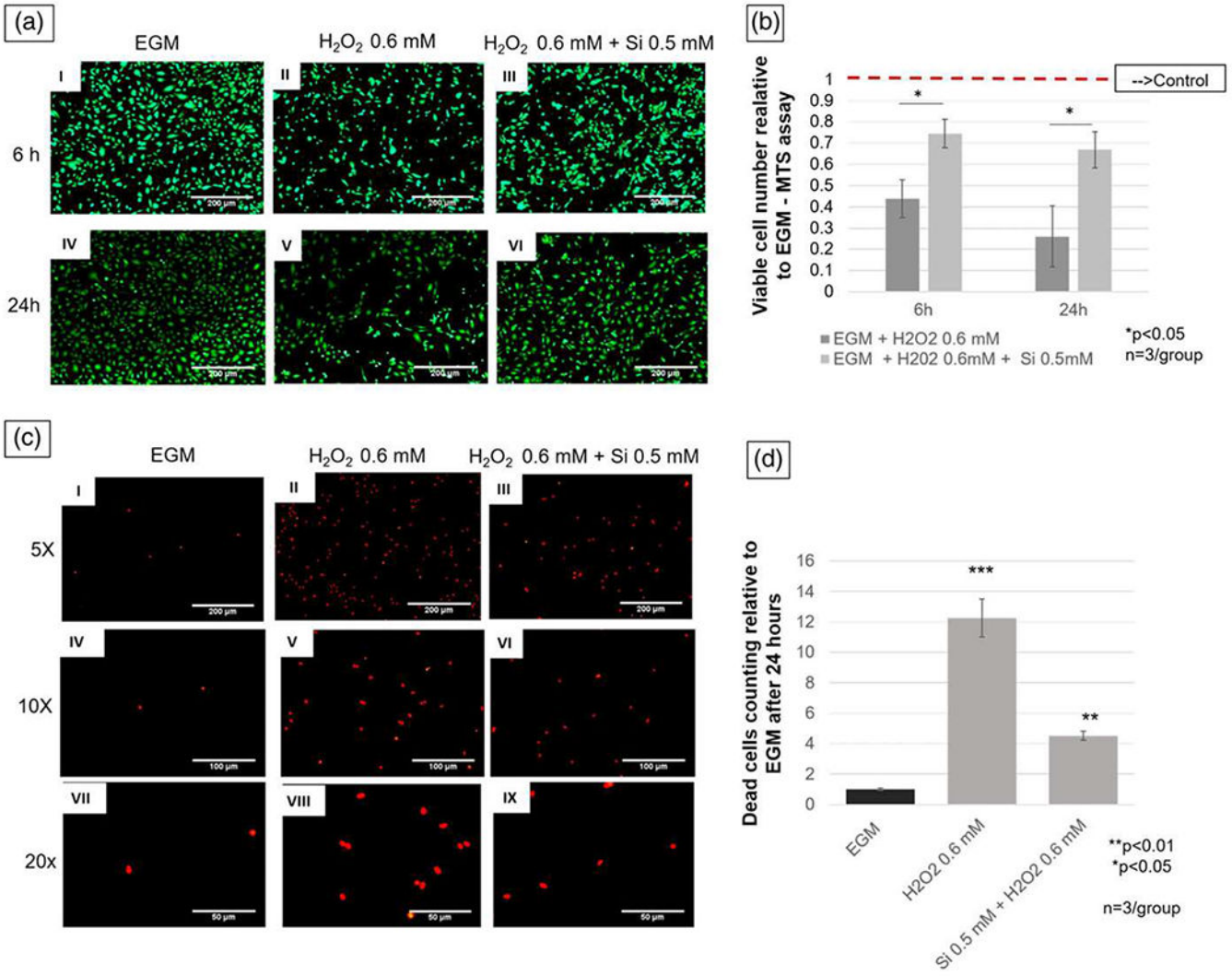

FIGURE 5.

(a) Pictures (5× view) of human umbilical vein endothelial cells stained with Calcein-AM under hydrogen peroxide oxidative stress with and without silicon ion treatment, as compared with control. Pictures I and IV show EGM (control) group. Pictures II and V show cells exposed to H_2O_2, and pictures III and VI show human umbilical vein endothelial cells under H_2O_2 environment and treated with Si^{4+} 0.5 mM (scale bar = 200 μm). (b) Graph presents data of comparison between treated and nontreated group relative to control (EGM). Treatment group shows twice and three times more viable cells than H_2O_2 0.6 mM group at 6 and 24 hr, respectively. (c) Fluorescent pictures after propidium iodide staining 24 hr after cell seeding. Pictures I, IV, and VII show different magnification of lowest number of dead cells on negative control (EGM). Pictures II, V, and VIII show different magnifications of highest number of dead cells on positive control (H_2O_2 0.6 mM). Pictures III, VI, and IX show lower number of dead cells than positive control (5× view, scale bar = 200 μm; 10× view, scale bar = 100 μm; 20× view scale bar = 50 μm). (d) Bar graph shows that silicon treatment group (H_2O_2 + Si 0.5 mM) have three times less dead cells than positive control (H_2O_2 0.5 mM). ***$p < 0.001$, **$p < 0.01$, *$p < 0.05$ indicate statistical

significance; n = 3 per group). EGM: endothelial cell growth media [Colour figure can be viewed at wileyonlinelibrary.com]

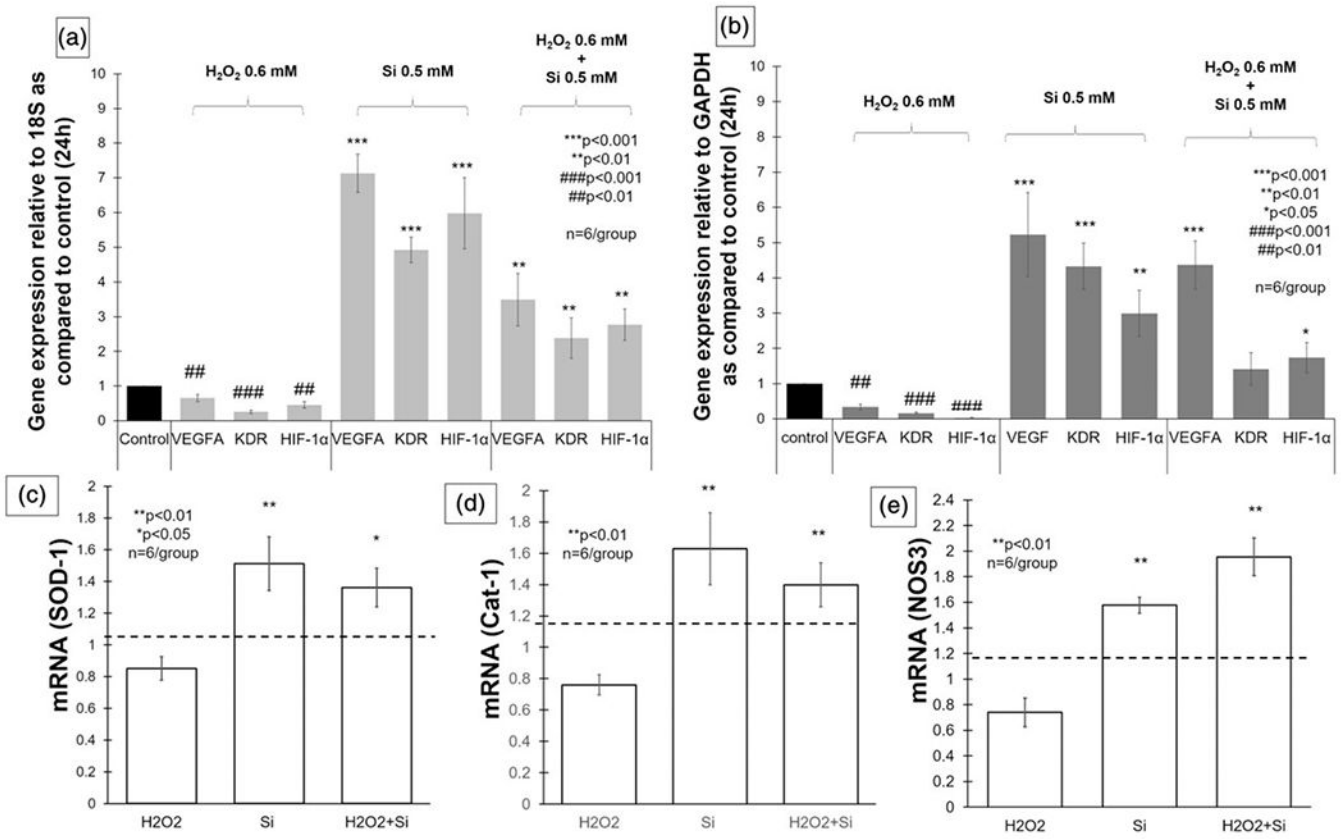

FIGURE 6.

Bar graphs showing gene expression after 24 hr. (a) VEGFA, KDR, and HIF-1α were significantly underexpressed when human umbilical vein endothelial cells were exposed to H_2O_2 0.6 mM ($p < 0.01$), and over expressed on silicon group ($p < 0.001$) and H_2O_2 treated with silicon group ($p < 0.01$) relative to 18S, as compared with control (EGM 20%). (b) Bar graph presenting gene expression of VEGFA, KDR, and HIF-1α, 24 hr after cell seeding relative to GAPDH, as compared with control (EGM 20%). VEGFA, KDR, and HIF-1α underexpressed on H_2O_2 0.6 mM ($p < 0.01$) and presented significant overexpression on silicon group ($p < 0.01$). VEGFA ($p < 0.001$) and HIF-1α ($p < 0.05$) were significantly increased on cells exposed to H_2O_2 and treated with silicon. (c–e) Bar graphs showing gene expression of SOD-1, Cat-1, and NOS-3 relative to 18S and compared with control. The three enzymes were significantly overexpressed, when exposed to ionic silicon with and without H_2O_2 (ANOVA, $^{**}p < 0.01$, $^{*}p < 0.05$ indicate statistical significance; $n = 6$ per group). VEGFA: vascular endothelial growth factor-A; KDR (VEGFR-2): vascular endothelial growth factor receptor 2; HIF-1α: hypoxia-inducible factor 1-alpha; GAPDH: glyceraldehyde 3-phosphate dehydrogenase; EGM: endothelial cell growth media; SOD-1: superoxide dismutase-1; Cat-1: catalase-1; NOS3: nitric oxide synthase-3

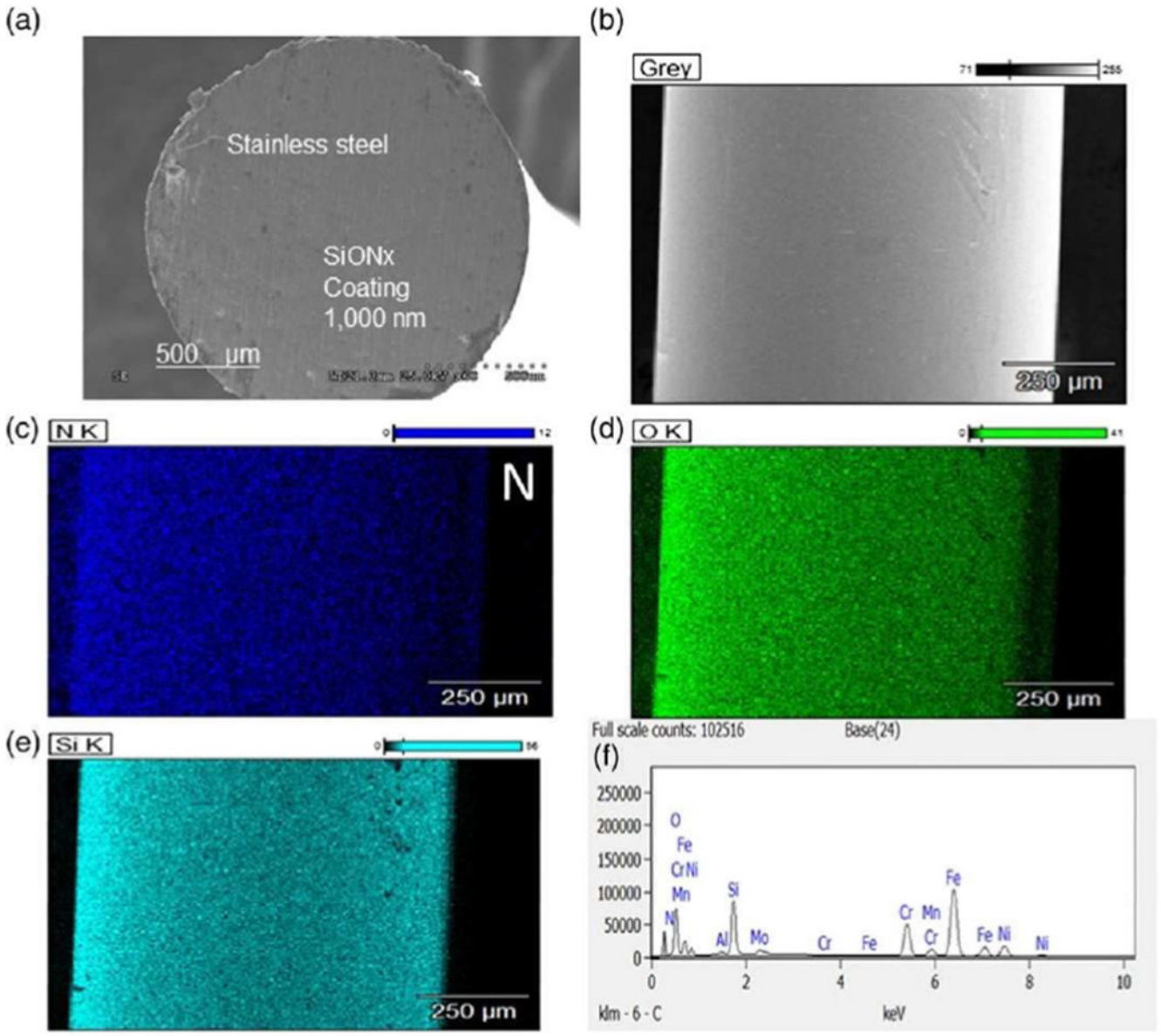

FIGURE 7.

$SiON_x$ fabricated onto 3D surgical stainless steel. Cross-sectional scanning (a) and topographical (b) electron micrograph showing the fabricated $SiON_x$ coating on surgical stainless rod showing homogeneity of silicon, oxygen, and nitrogen (c–f) throughout the coating [Colour figure can be viewed at wileyonlinelibrary.com]

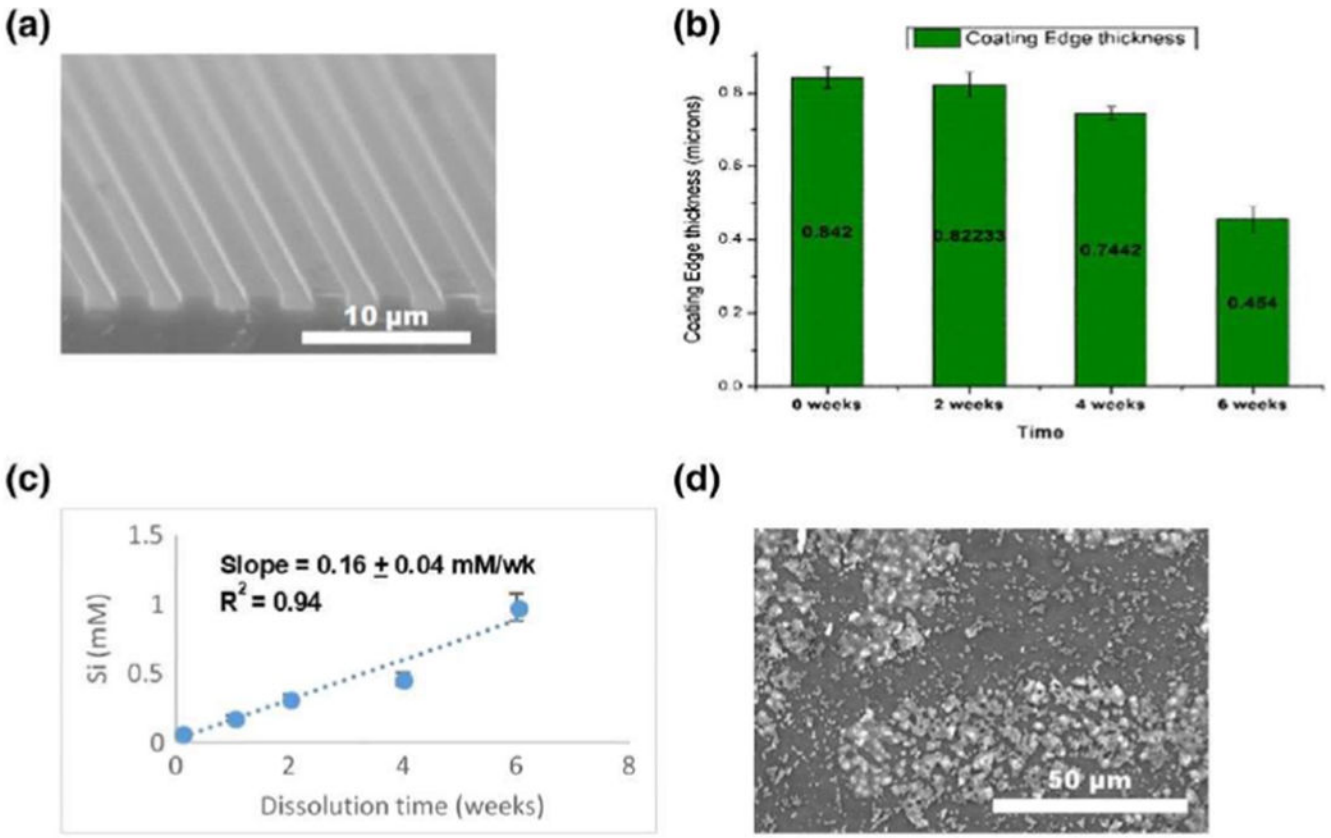

FIGURE 8.

$SiON_x$ coatings on implant surfaces (a) was immersed in alpha-MEM for 6 weeks. The coating was observed to degrade over 6 weeks (b) and estimated for the approximate rate of ionic Si release (c). The resultant surface appeared to have the formation of hydroxyapatite crystals in a c-axis orientation (d) [Colour figure can be viewed at wileyonlinelibrary.com]

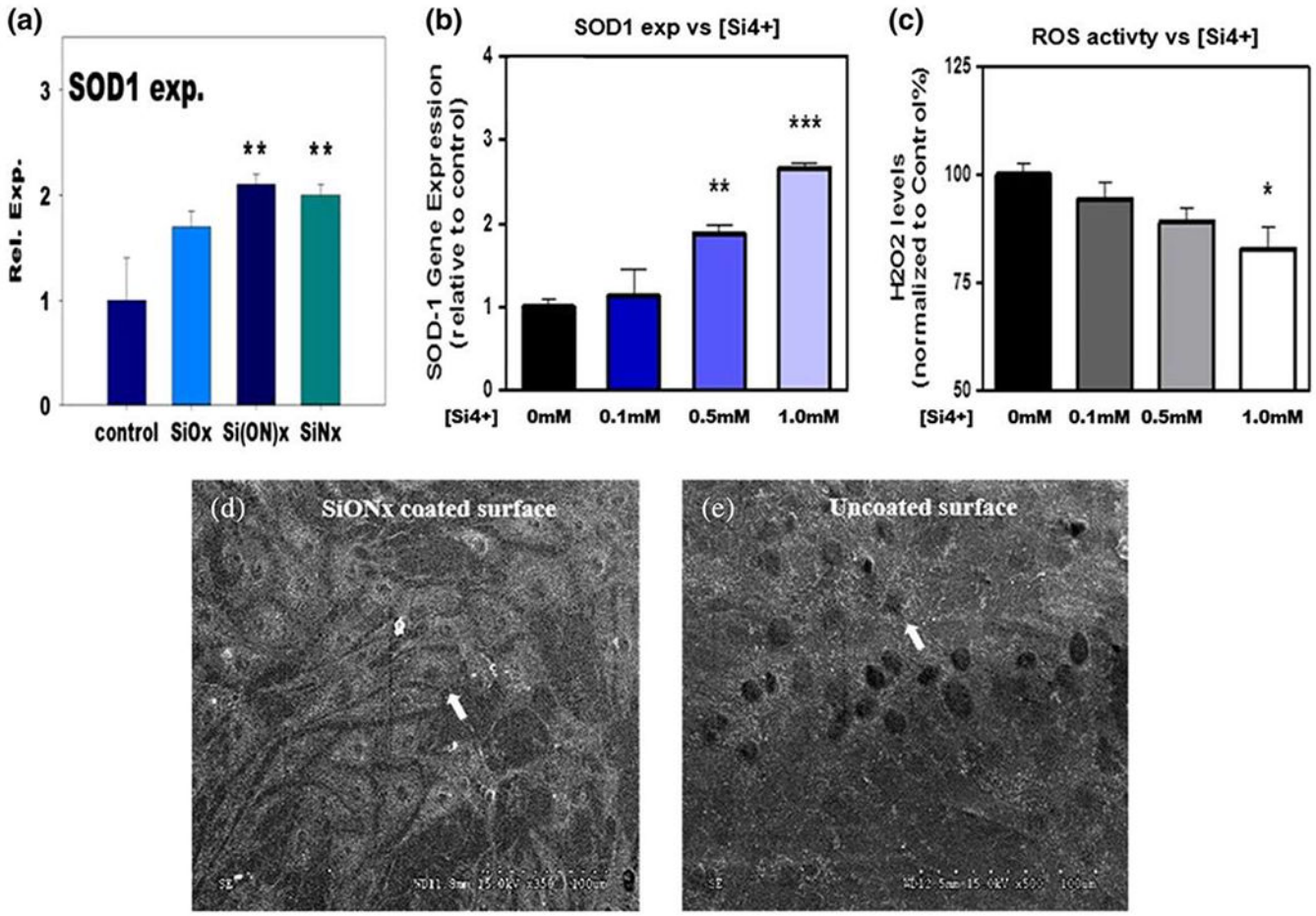

FIGURE 9.

$SiON_x$ and ionic Si enhance osteo-progenitor and angio-progenitor functions. Enhanced antioxidant SOD-1 expression in differentiated human periosteum cells within 3–4 days (a). The ionic Si was also found to enhance SOD-1 gene expression (b) and reduce ROS levels (c) in endothelial cell culture within 24 hr. Porcine endothelial cells density on $SiON_x$ surfaces (d) was higher and more elongated than on uncoated implant surfaces (e). White arrows show endothelial cells (ANOVA, * $p < 0.05$, ** $p < 0.01$, *** $p < 0.001$ indicate statistical significance). SOD: superoxide dismutase; ROS: reactive oxygen species [Colour figure can be viewed at wileyonlinelibrary.com]

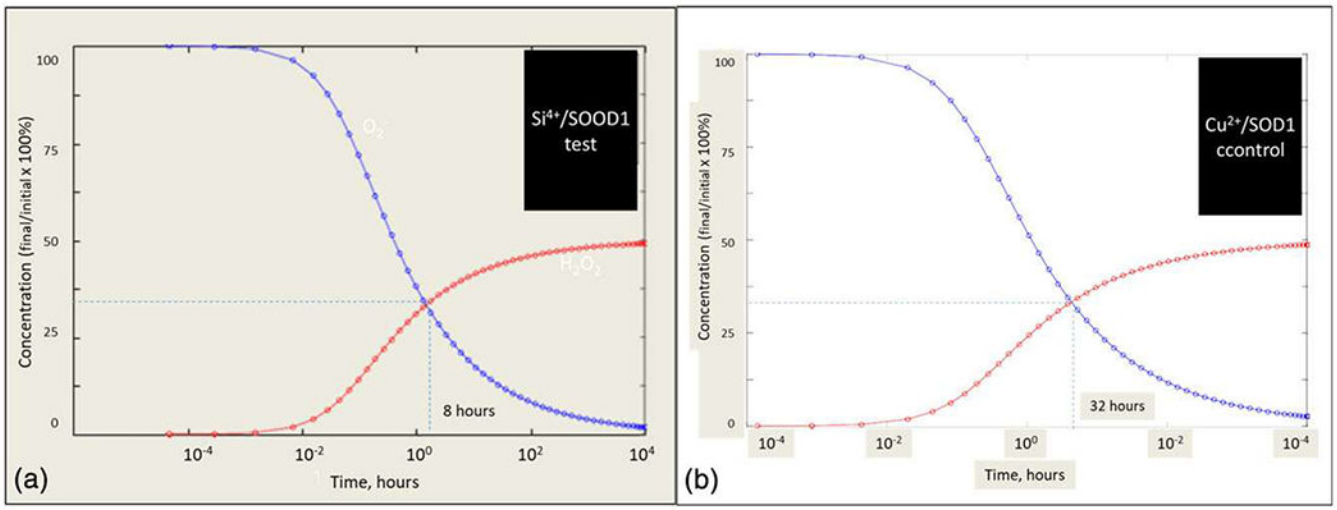

FIGURE 10.

Calculated conversion of superoxide anion to H_2O_2 via Si induced (a) and control (b) SOD-1 expression. The equilibrium reaction, $O_2^- + 2H+ = H_2O_2$, was used for the base equilibrium reaction, and the addition of ionic Si versus Cu was compared. The use of a mass action model with the valence state of the element used a variable for the rate of reaction. It was found that an increase from 2+ valence to 4+ valence was found to reach equilibrium concentration of the reaction by a factor of 4 (from 32 to 8 hr). SOD: superoxide dismutase [Colour figure can be viewed at wileyonlinelibrary.com]

TABLE 1

Gene and specific TagMan® assay ID

Gene	Assay ID
VEGFA	Hs00900055_m1
VEGFR-2 (KDR)	Hs00911700_m1
HIF1-α	Hs00153153_m1
SOD-1	Hs00533490_m1
Cat-1	Hs00156308_m1
NOS3	Hs01574665_m1
18S	Hs03003631_g1
GAPDH	Hs02786624_g1

TABLE 2

System of non-linear differential equations that make up mass action enzymatic model used in Figure 10

Test condition: Si/DOD1

Overall Reaction:

$$Si^{4+} SOD1 + 6O_2^{-+} + 6H^{+-} \rightarrow Si^{4+} SOD1 + 3H_2O_2 + 3O_2$$

Modelled reaction:

$$6O_2^{-} + 6H^{+-} \rightarrow 3H_2O_2 + 3O_2$$

System of modelled reaction equations:

$$d\frac{O_2]^{-}}{\mathrm{dt}} = -6[O_2^{-}]^2[H^{+}]^2k_{+}$$

$$\frac{d[H^{+}]}{\mathrm{dt}} = -6[O_2^{-}]^2[H^{+}]^2k_{+}$$

$$\frac{d[H_2O_2]}{\mathrm{dt}} = 3[O_2^{-}]^2[H^{+}]^2k_{+}$$

$$\frac{d[O_2]}{\mathrm{dt}} = 3[O_2^{-}]^2[H^{+}]^2k_{+}$$

Control: Cu/SOD-1

Overall reaction:

$$\mathrm{Cu}^{2+} SOD1 + 2O_2^{-} + 2H^{+-} \rightarrow \mathrm{Cu}^{2+} SOD1 + H_2O_2 + O_2$$

Modelled reaction:

$$2O_2^{-} + 2H^{+-} \rightarrow H_2O_2 + O_2$$

System of model reaction equations:

$$d\frac{O_2]^{-}}{\mathrm{dt}} = -2[O_2^{-}]^2[H^{+}]^2k_{+}$$

$$\frac{d[H^{+}]}{\mathrm{dt}} = -2[O_2^{-}]^2[H^{+}]^2k_{+}$$

$$\frac{d[H_2O_2]}{dt} = [O_2^-]^2[H^+]^2 k_+$$

$$\frac{d[O_2]}{dt} = [O_2^-]^2[H^+]^2 k_+$$